IVYSPRING INTERNATIONAL PUBLISHER

Theranostics

2019; 9(14): 4047-4065. doi: 10.7150/thno.33228

Review

Chemiluminescence and Bioluminescence Imaging for Biosensing and Therapy: *In Vitro* and *In Vivo* Perspectives

Yongcun Yan[1,4], Pengfei Shi[1,3], Weiling Song[2], Sai Bi[1,3,4]✉

1. Center for Marine Observation and Communications, Research Center for Intelligent and Wearable Technology, College of Chemistry and Chemical Engineering, Qingdao University, Qingdao 266071, P. R. China
2. Laboratory of Optic-electric Sensing and Analytical Chemistry for Life Science, MOE, Shandong Key Laboratory of Biochemical Analysis; Key Laboratory of Analytical Chemistry for Life Science in Universities of Shandong; College of Chemistry and Molecular Engineering, Qingdao University of Science and Technology, Qingdao 266042, P. R. China
3. Collaborative Innovation Center of Tumor Marker Detection Technology, Equipment and Diagnosis-Therapy Integration in Universities of Shandong, Shandong Province Key Laboratory of Detection Technology for Tumor Markers, College of Chemistry and Chemical Engineering, Linyi University, Linyi 276000, P. R. China
4. Jinan Guoke Medical Engineering Technology Development Co., Ltd., Jinan 250101, P. R. China

✉ Corresponding author: E-mail address: bisai11@126.com

© Ivyspring International Publisher. This is an open access article distributed under the terms of the Creative Commons Attribution (CC BY-NC) license (https://creativecommons.org/licenses/by-nc/4.0/). See http://ivyspring.com/terms for full terms and conditions.

Received: 2019.01.17; Accepted: 2019.04.25; Published: 2019.05.31

Abstract

Chemiluminescence (CL) and bioluminescence (BL) imaging technologies, which require no external light source so as to avoid the photobleaching, background interference and autoluminescence, have become powerful tools in biochemical analysis and biomedical science with the development of advanced imaging equipment. CL imaging technology has been widely applied to high-throughput detection of a variety of analytes because of its high sensitivity, high efficiency and high signal-to-noise ratio (SNR). Using luciferase and fluorescent proteins as reporters, various BL imaging systems have been developed innovatively for real-time monitoring of diverse molecules *in vivo* based on the reaction between luciferin and the substrate. Meanwhile, the kinetics of protein interactions even in deep tissues has been studied by BL imaging. In this review, we summarize *in vitro* and *in vivo* applications of CL and BL imaging for biosensing and therapy. We first focus on *in vitro* CL imaging from the view of improving the sensitivity. Then, *in vivo* CL applications in cells and tissues based on different CL systems are demonstrated. Subsequently, the recent *in vitro* and *in vivo* applications of BL imaging are summarized. Finally, we provide the insight into the development trends and future perspectives of CL and BL imaging technologies.

Key words: chemiluminescence, bioluminescence, bioimaging, biosensing, biomedicine

1. Introduction

Chemiluminescence (CL), as a widely used photon emission-based analytical technique, has developed rapidly from the late 1970s [1]. CL can be described as the phenomenon of emitting photons when electrons return from the excited state to the ground state during a chemical reaction. Compared with traditional detection techniques, the most remarkable advantage of CL is the high sensitivity resulted from no need of an external light source. Therefore, CL can reduce the light scattering, improve SNR and detection sensitivity, and expand the linear dynamic range. Since horseradish peroxidase (HRP) was first reported to catalyze the oxidation of luminol by H_2O_2, the CL signals were amplified extremely and the CL assays were also developed increasingly. In addition to luminol, many CL substrates, such as acridinium ester, peroxyoxalate, 1,2-dioxetane and their derivatives, have been found. With the development of CL systems and advanced analytical equipment with high resolution such as photomultiplier tube and charge-coupled device (CCD), CL imaging technology has become attractive in *in vitro* and *in vivo* applications [2, 3]. To get better imaging effect, CCD-based imaging devices have

become more and more popular [4]. Slow-scan CCD detectors are suitable for steady-state CL signal with a high quantum effect [5]. Meanwhile, cryogenic freezing technology can reduce noise and promote SNR. Further, intensified CCD and imaging photon detectors provide high sensitivity in CL detection [6]. At present, the commercial development of CCD devices with high sensitivity and high resolution makes the application of CL imaging more widely. It is easy to measure photon signals in microarrays to achieve simultaneous analysis of multicomponent substances, in which the amounts of the samples are greatly reduced. Up to now, CL imaging technology has been applied to detect a wide range of analytes in the field of biochemical analysis, including nucleic acids, proteins, enzymes, small biological molecules, and even cells [7, 8].

To monitor the diverse *in vivo* processes such as tumor growth, drug delivery and pathogen shifts, practicable and high-resolution optical imaging technologies have been developed [9]. In particular, *in vivo* CL imaging has great significance for evaluation of cell and animal models and real-time monitoring of physiology and pathology processes [10]. With the continuous progress of novel CL materials and optical detection technologies, the research on CL imaging will be further expanded, and the existing limitations, such as the precision of target localization, will be broken.

In view of the weak tissue penetration and short timeliness of *in vivo* CL imaging models, some important physiological and pathological processes in living systems cannot be monitored, especially in deep tissues [11]. Alternatively, bioluminescence (BL) imaging has become one of the most popular noninvasive *in vivo* tools in the past decade. BL is generated via enzymatic reaction through the conversion of chemical energy into light in living organism without excitation source. In a typical BL reaction, luciferase catalyzes the oxidation of the substrate (e.g., luciferin). So far, a variety of luciferases are used in BL systems and many of them can be used to in-depth image cells and tissues [12]. For example, the most striking NanoLuc can offer enhanced stability which has smaller size than Firefly and *Renilla* luciferases [13]. Due to its good biocompatibility and persistence, BL imaging has been used to monitor gene expression, cellular and intracellular motility, protein interactions in cells, tissues and organs [14]. Because of the diversity of the luciferase-luciferin pairs in BL systems, BL imaging has achieved simultaneous determination of multi-components. Based on the unique properties, the penetration, specificity and persistence of *in vivo* BL systems have been greatly improved. To obtain higher sensitivity, redesigned luciferase mutants and luciferin analogs are also emerging [15].

As mentioned above, both CL and BL are well-established photon emission-based detection technologies, which hold the advantages in terms of no requirement of external light source and avoiding the photobleaching, background interference and autoluminescence. Thus, CL and BL have achieved high sensitivity and wide application ranges. In this review, the *in vitro* and *in vivo* applications of CL and BL imaging technologies are overviewed. Although some review articles have been previously published on CL and BL imaging, most of them focused on the *in vitro* CL imaging assays based on traditional CL systems as well as the *in vivo* BL imaging using common luciferase-luciferin pairs. However, the *in vivo* CL imaging and retooling BL systems are rarely mentioned. In this review, we first summarize the recent research advances of *in vitro* CL imaging from the perspective of the improvement of detection sensitivity. Then, the development and applications of *in vivo* CL imaging are introduced. Moreover, the *in vivo* BL imaging systems are summarized, including in situ formation of luciferase and luciferase mutants for BL imaging, in situ formation of luciferin and luciferin analogs for BL imaging, and bioluminescence resonance energy transfer (BRET) imaging. Finally, the limitations and future perspectives of CL and BL imaging technologies are provided.

2. *In vitro* CL imaging

As a powerful optical technique, CL imaging has been versatilely applied in *in vitro* detection of a wide range of analytes, such as nucleic acids, proteins, small molecules and even cells [16]. Up to now, some reviews about CL imaging have been published, which were summarized on the basis of analytical formats such as microtiter plates and microarrays [2] or according to the analytes [17]. However, at present the major challenge of *in vitro* CL imaging is how to improve the detection sensitivity. Therefore, we summarize the recent research advances of *in vitro* CL imaging from three representative parts regarding to improve the sensitivity: nanoprobe-based CL imaging for signal amplification, isothermal amplification-based CL imaging assays, and integrated CL imaging devices.

2.1. Nanoprobe-based CL imaging for signal amplification

To improve the detection sensitivity, novel CL probes have been explored and applied in CL imaging [6, 18-20]. For example, gold nanoparticles (AuNPs) have been widely used as labels for signal

amplification [21-23]. Through binding HRP molecules to AuNPs with a high loading ratio [24], CL imaging platforms have been developed for the detection of various tumor markers [25-27], achieving cancer screening with high throughput, good reproducibility and high accuracy. Meanwhile, using HRP-labeled AuNPs as nanoprobes, human cancer cells were imaged and the glycan expression on cell surface was monitored (**Figure 1A**) [28]. In particular, because of the high chemical stability, enhanced catalytic activity and low cost in comparison with HRP molecules, G-quadruplex/hemin HRP-mimicking DNAzyme has been widely used in biochemical analysis [29, 30]. Ju's group developed a CL imaging immunoassay using multilayer hemin/G-quadruplex coated AuNPs as probes for simultaneous detection of multiple antigens with ultrahigh sensitivity [25].

Recently, bio-bar-code AuNP probes have proven to be able to significantly improve the detection sensitivity through efficiently avoiding cross reaction [31-33]. In the construction of bio-bar-code probes, AuNPs as carriers are functionalized with both bar-code DNAs and specific identification elements such as antibody and aptamer with a ratio of n:1, which thus decreases the recognition reaction from one-to-many to one-to-few and realizes signal amplification [34]. Through combining CL imaging array and bio-bar-code AuNPs, Bi et al. realized the ultrasensitive detection of human Burkitt's lymphoma cells with a LOD as low as 163 cells (**Figure 1B**) [35].

Inorganic luminescent nanomaterials with high photo-intensity were also used in CL imaging systems as novel probes. Quantum dots (QDs) are a class of semiconductor nanomaterials with adjustable emission spectra and long fluorescence life so that they are suitable for the construction of luminescent probes in CL imaging assays. In particular, nitrogen-doped graphene quantum dots (NGQDs) with excellent light stability have been used as luminescence probes for ascorbic acid detection based on the catalysis of copper ion [36].

In addition, polymers have also been employed as probes in CL imaging assays. Through using molecularly imprinted polymers as recognition probes, the selectivity of CL imaging has been significantly improved [37-39], achieving sensitive and specific detection of a variety of small organic molecules, such as 2,4-dichlorophenoxyacetic acid [40], trans-resveratrol [41], dipyridamole [42] and dansyl-phenylalanine [43]. Recently, using folic acid and HRP-bifunctionalized semiconducting polymer dots as integrated probes, a CL platform was developed for imaging of cancer cells and targeted photodynamic therapy (PDT) of tumors via chemiluminescence resonance energy transfer (CRET) (**Figure 1C**) [44].

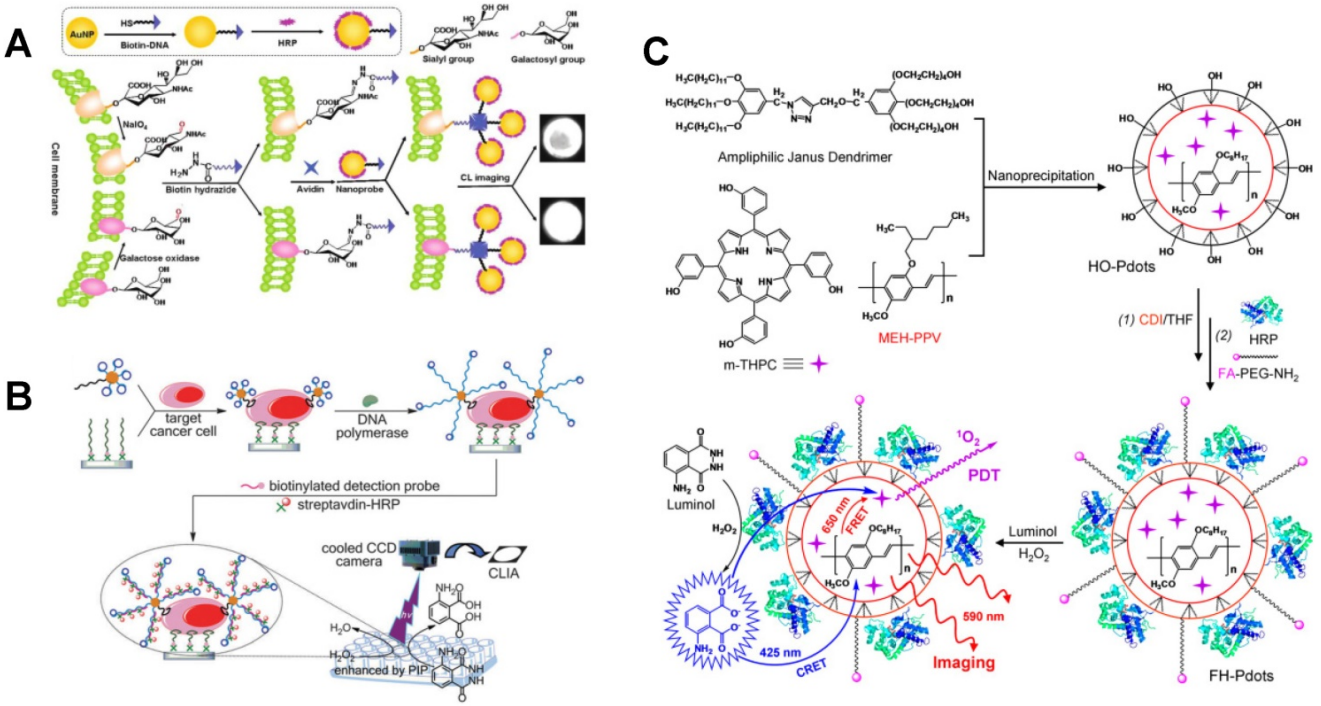

Figure 1. CL imaging of cancer cells using multifunctional nanoprobes. (A) Glycan expression-based CL imaging of HCCC-9810 cells using AuNP probes. Reprinted with permission from [28], Copyright 2012, American Chemical Society. **(B)** Dual-aptamer recognition-based CL imaging of Ramos cells using bio-bar-code AuNP probes. Reprinted with permission from [35], Copyright 2013, Royal Society of Chemistry. **(C)** Folic acid and HRP-bifunctionalized semiconducting polymer dots for both CL imaging and PDT of tumor cells. Reprinted with permission from [44], Copyright 2014, American Chemical Society.

2.2. Isothermal amplification-based CL imaging assays

As a commonly used molecular biology technique for amplification, polymerase chain reaction (PCR) has been widely used in diagnosis of diseases due to its high amplification efficiency. So far, a variety of PCR-based CL imaging strategies have been developed for biomolecular analysis [45-49]. However, PCR often suffers from the disadvantages of complicated temperature control and nonspecific amplification. Alternatively, isothermal amplification strategies, such as tool enzyme-assisted signal amplification methods [50-53] and toehold-mediated strand displacement reaction [54], have been versatilely applied in CL imaging of nucleic acids [50, 51, 55, 56], cancer cells [35] and bacteria [52]. For example, Seidel et al. developed a flow CL imaging microarray MCR 3 based on recombinase polymerase amplification (RPA) for multiplex detection of viral and bacterial DNA (**Figure 2A**) [52]. This on-chip isothermal nucleic acid amplification test (iNAAT) was performed at a constant temperature of 39 °C. After immobilizing HRP molecules on the chip via specific interaction between biotin and strepavidin, HRP catalyzed the CL reaction of luminol-H_2O_2 and the signals were collected by a CCD camera for CL imaging.

In addition, through combining DNA polymerase/nicking enzyme-assisted molecular machine with programmable toehold-mediated strand displacement reactions, a CL imaging array was reported for simultaneous detection of three miRNAs with high throughput (**Figure 2B**) [57]. In this assay, three kinds of hairpins were immobilized on magnetic particles. The introduction of different target miRNAs initiated the DNA machine in the presence of Klenow exo- polymerase and Nb.BbvCI nicking enzyme, resulting in the displacement of target miRNAs and the generation of a large number of single-stranded DNAs to trigger another DNA machine. After sequential addition of three displacement probes, HRP-tagged DNA strands were released from magnetic particles based on toehold-mediated strand displacement, achieving simultaneous CL imaging of three miRNAs (miR-155, miR-let-7a and miR-141) with the detection limits as low as fM level.

2.3. Integrated CL imaging devices

In recent years, many miniaturized and integrated CL imaging devices, such as microfluidic cloth-based analytical devices (μCADs), have been developed for small molecule detection [58, 59]. In addition, a variety of CL imaging devices have been reported for efficient and sensitive analysis of proteins, such as microfluidic-based chips [60], lateral flow-based disposable cartridge [61], capillary isoelectric focusing immunoassay [63], paper-based microfluidic sensor [64], and 3D printing-based all-in-one immuno-device (**Figure 3**) [62]. With the continuous development of imaging equipment and techniques, scanning CL microscopy (SCLM) has been developed [65, 66]. Moreover, scanning electrochemical microscopy (SECM) was combined with luminescence technique [67]. For example, SECM/electrogenerated chemiluminescence (ECL) setup was established and applied for the detection of enzyme activity [68]. The automation of these devices dramatically shortened the operation time and improved sensitivity, which can be versatilely applied in clinical diagnosis.

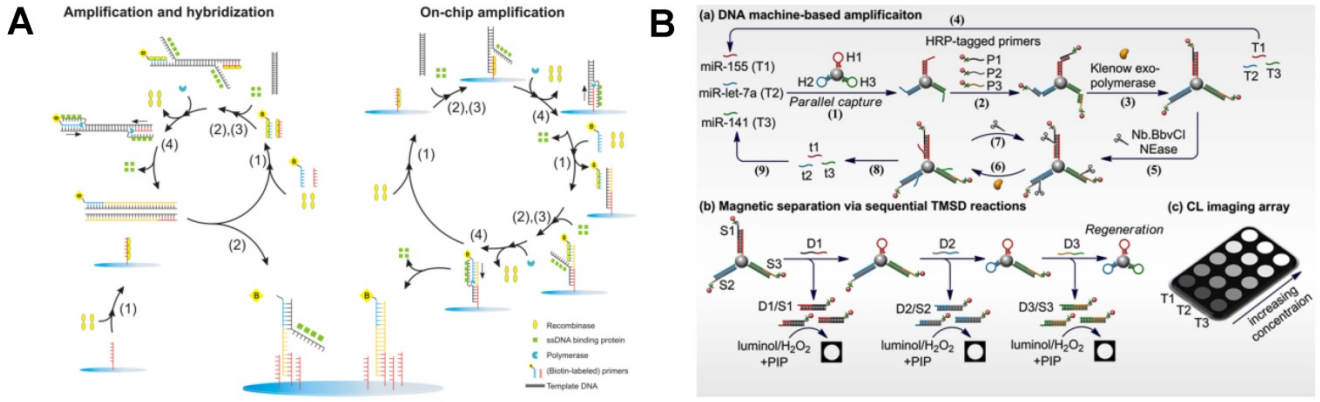

Figure 2. Tool enzyme-based isothermal amplification for CL imaging of nucleic acids. (A) Automated on-chip CL imaging platform based on RPA for simultaneous detection of viruses and bacteria. Reprinted with permission from [52], Copyright 2016, American Chemical Society. **(B)** CL imaging for simultaneous amplified detection of three microRNAs via programmable strand displacement-based magnetic separation. Reprinted with permission from [57], Copyright 2017, Elsevier B.V.

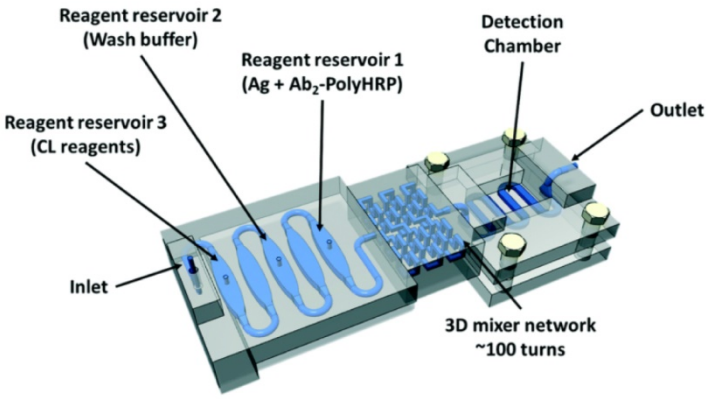

Figure 3. The structure of 3D-printed unibody immunoarray for detection of PSA and PF-4. Reprinted with permission from [62], Copyright 2017, Royal Society of Chemistry.

3. *In vivo* CL imaging

To better understand the gene expression, pathogenesis and treatment of diseases in depth, intracellular and intra-tissue imaging are essential. With the development of the optical equipment, CL has been well advanced from *in vitro* imaging to *in vivo* imaging. To resolve the problem of light transmittance and tissue self-absorption during CL imaging *in vivo*, novel and biocompatible CL probes have been fabricated, such as multifunctional polymer nanoparticles (NPs) [69] and near-infrared (NIR) fluorescent dyes [70-72]. It should be noted that the NIR fluorescence generated from these fluorescent dyes is not direct CL emission but the non-radiative energy transfers from the CL substrate to fluorescent receptor which can emit at NIR region. Meanwhile, *in vivo* CRET systems have been developed to enhance the CL emission using fluorescein, QDs, AuNPs, graphene and graphene oxide (GO) as the energy acceptors. All of these meaningful improvements have led to the excellent sensitivity and high accuracy of *in vivo* CL imaging [73-76].

3.1. Peroxyoxalate chemiluminescence (POCL) polymer-based CL imaging

Unlike *in vitro* detection, tissue self-absorption and low penetrability limit the application of traditional CL imaging systems in *in vivo* imaging. In view of this, novel CL imaging probes were fabricated. Using peroxyoxalate and corresponding polymer NPs, nonenzymatic POCL systems have been developed and widely applied for *in vivo* CL imaging assays, in which the oxidation of the probes and the generation of high-energy dioxetanedione intermediate excited the fluorescent dyes. Meanwhile, the CL color is adjustable through changing the fluorescent dyes in the polymer NPs. Lee et al. first applied POCL NPs (emitted at 630 nm) to image exogenous H_2O_2 in mice's leg, achieving a detection sensitivity as low as 250 nM for H_2O_2 [77]. To reduce the self-absorption of tissue, another all-in-one peroxyoxalate NPs with NIR CL were proposed by Kim's group [10]. The CL substrate bis[3,4,6-trichloro-2-(pentyloxycarbonyl)phenyl] oxalate (CPPO) reacted with H_2O_2 and generated the 1,2-dioxetanedione intermediate. Then the encapsulated NIR dye 3,3'-diethylthiadicarbocyanine iodide (Cy5) was excited by 1,2-dioxetanedione with the maximum emission at 701 nm. In addition to H_2O_2, glucose level was also detected using this peroxyoxalate NP-based CL imaging strategy. Recently, Kim et al. improved the peroxyoxalate NPs to enhance the intensity and adjustability of CL in imaging H_2O_2 [78]. As shown in **Figure 4A**, a green-emitting dye of 9,10-distyrylanthracene derivative (BLSA) was synthesized to fabricate the NPs and the CL signals from the BLSA/CPPO aggregates can be enhanced by aggregation-enhanced fluorescence. In particular, when doped with a secondary energy acceptor Nile Red, CL would change from green to red through energy transfer, which realized tunable CL for sensitive imaging of H_2O_2 and inflammation.

Through encapsulating therapeutic agents, POCL polymer NPs can not only image small molecules but also treat correlative diseases. For example, a chemiluminescent and antioxidant micelle was designed to detect H_2O_2 *in vivo* as well as to encapsulate therapeutic agents for H_2O_2-associated inflammatory diseases [79]. **Figure 4B** showed that the fluorescent dyes and hydroxybenzyl alcohol-incorporated copolyoxalate (HPOX) were encapsulated in the amphiphilic block copolymer pluronic F-127 to constitute the micelle, which was then applied to detect and treat lipopolysaccharide (LPS)-induced inflammation in mouse ankles. The overproduced H_2O_2 participated in the POCL reaction and as low as 100 nM H_2O_2 can be imaged in the inflamed ankles. Furthermore, the antioxidant micelle can scavenge the overproduced H_2O_2 availably and release therapeutic antioxidant hydroxybenzyl

alcohol. Therefore, this CL antioxidant micelle showed curative effect to H_2O_2-induced inflammation and apoptosis. Moreover, a multifunctional POCL polymer NPs-based probe was synthesized for both CL imaging of H_2O_2 and tumor therapy [80]. CPPO and aggregation-induced emission photosensitizer of TPE-BT-DC (TBD) were co-encapsulated using F-127 and soybean oil via precipitation. After intravenous administration, the as-synthesized C-TBD NPs could preferentially accumulate in the tumor region because of the enhanced permeability and retention effect. Then, the C-TBD NPs emitted at far-red/NIR region and the strong red emission was observed by the naked eye, realizing tumor tracking. Meanwhile, the TBD in C-TBD NPs would generate $^1O_2$ efficiently, which could lead to the apoptosis of tumor cells and realize the accurate and noninvasive tumor therapy. Further, β-phenylethylisothiocyanate was used to increase the H_2O_2 concentration in both tumor imaging and therapy.

Intragranular CRET or FRET in POCL polymer NPs can adjust CL emission to red shift and therefore improve the ability of light to penetrate tissue. Rao et al. monitored the drug-induced ROS and reactive nitrogen species simultaneously by combining CRET with FRET in the liver of living mice (**Figure 5A**) [81]. Semiconducting POCL polymer NPs were synthesized with two polymers for real-time monitoring the stress changes of $ONOO^-$ and H_2O_2 caused by anti-pyretic acetaminophen and anti-tuberculosis agent isoniazid. In the synthesis of this CRET-FRET-polymer NPs (CF-polymer NPs), poly(2,7-(9,9-dioctylfluorene)-alt-4,7-bis(thiophen-2-yl)benzo-2,1,3-thiadiazole) acted as the FRET donor and the CRET acceptor, in which CPPO was the CL substrate for H_2O_2 and a cyanine dye was used for the fluorescence-based sensor. Meanwhile, a galactosylated graft copolymer PS-g-PEG-Gal was modified on the CF-polymer NPs, which can target the CF-polymer NPs to the liver accurately. The imaging of hepatotoxicity can be completed within minutes and the LOD for CL imaging of H_2O_2 was 5 nM. To monitor H_2O_2 concentration *in vivo* with higher sensitivity, the intensity and stability of CL light emission as well as the visualization of imaging have been improved. Pu et al. synthesized another kind of semiconducting POCL polymer NPs for the amplification of CL signals through facilitating electron transfer between molecules (**Figure 5B**) [82]. The semiconducting POCL polymer NPs was synthesized by coprecipitating bis(2,4,6-trichlorophenyl) oxalate (TCPO) with different polyfluorene-based semiconducting polymers and PEG-*b*-PPG-*b*-PEG. Further, a naphthalocyanine dye was doped into the POCL polymer NPs to generate NIR luminescence via intraparticle CRET between the CL substrate and the luminescence reporter. The results showed that the CL quantum yields were related to the energy difference, and the CL efficiencies of these polymer NPs were irrelevant to their fluorescence quantum yields. Among five polyfluorene-based semiconducting polymers, PFPV-based polymer NPs had the highest fluorescence intensity. Thus, PFPV was chosen as the luminescent reporter. This method achieved sensitive imaging of H_2O_2 that was related to peritonitis and neuroinflammation in mice. Recently, poly(phenylenevinylene) (PPV) was observed with continuous afterglow luminescence after removal of light source. So PPV-based semiconducting polymer NPs were synthesized via nano-coprecipitation, which realized the photothermal therapy (PTT) of tumors and monitored the photothermal temperature using afterglow imaging [83].

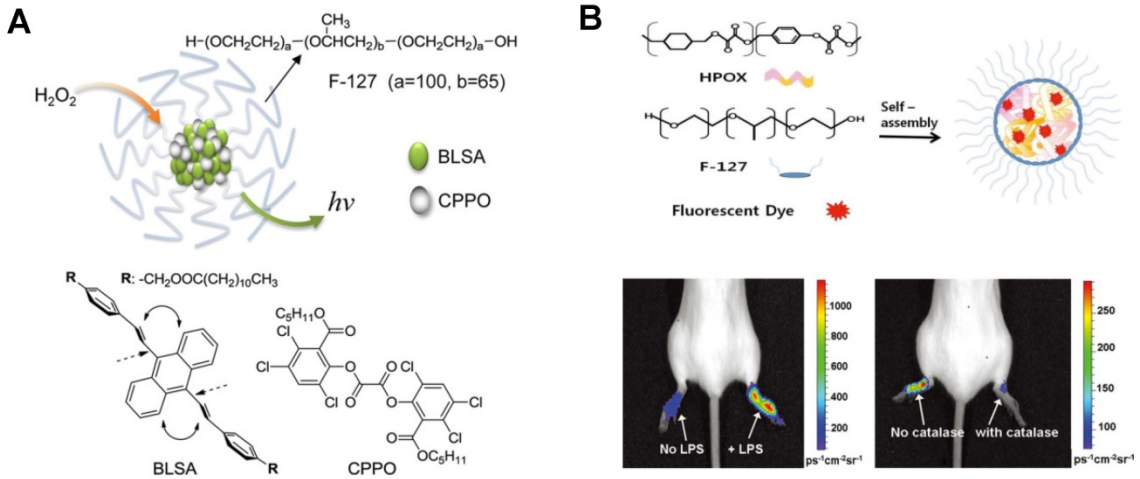

Figure 4. Polymer NPs-based CL imaging of *in vivo* H_2O_2. (A) BLSA/CPPO NPs with aggregation-enhanced fluorescence for CL imaging of H_2O_2. Reprinted with permission from [78], Copyright 2012, American Chemical Society. **(B)** Synthesis and application of HPOX micelles in H_2O_2 imaging. Reprinted with permission from [79], Copyright 2012, Wiley-VCH.

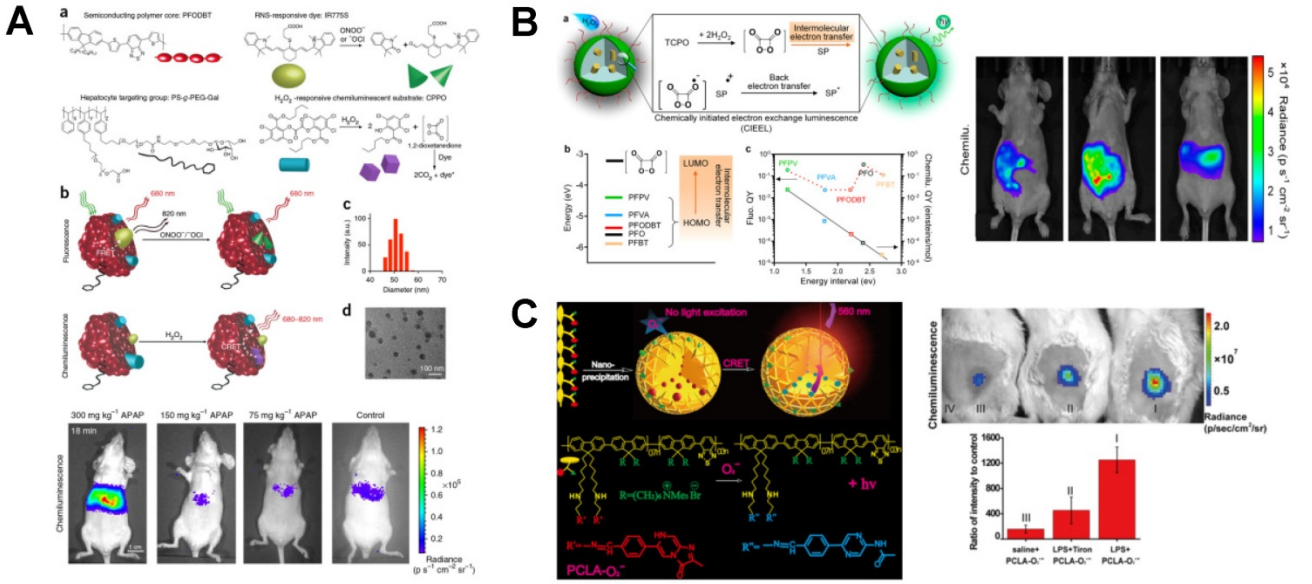

Figure 5. POCL polymer NPs-based CRET systems for *in vivo* H_2O_2 imaging. (A) Molecular components of CF-polymer NPs and the mechanism of $ONOO^-$/^-OCl and H_2O_2 detection by CF-polymer NPs. Reprinted with permission from [81], Copyright 2014, Nature Publishing Group. **(B)** Mechanism of the CRET in semiconducting POCL polymer NPs and the comparison between PFPV-based semiconducting POCL polymer NPs and other four semiconducting-based POCL polymer NPs, as well as *in vivo* CL imaging of endogenous H_2O_2 in the mouse model of neuroinflammation. Reprinted with permission from [82], Copyright 2016, American Chemical Society. **(C)** $O_2^{\bullet-}$ sensing and the structure of polymer PCLA-$O_2^{\bullet-}$, as well as the *in vivo* CL imaging of endogenous $O_2^{\bullet-}$. Reprinted with permission from [84], Copyright 2016, American Chemical Society.

Just like POCL probes for imaging H_2O_2, polymer polycaprolactone monoacrylate (PCLA) was also found to be an excellent material in CL imaging for the detection of $O_2^{\bullet-}$ in mice based on CRET [84]. As shown in **Figure 5C**, the polymer PCLA-$O_2^{\bullet-}$ nanoprobe was prepared by nanoprecipitation. Two segments of imidazopyrazinone and conjugated polymers (CPs) were connected through the covalent bond and they acted as the energy donor and acceptor, respectively. Once the $O_2^{\bullet-}$ was added, a radiationless energy-transfer was occurred from imidazopyrazinone to CPs with the emission of magnified light (λ_{max} = 560 nm). The utilizing of CRET eliminated some inherent shortcomings of CL in optical imaging, such as short emission time and wavelength. The PCLA-$O_2^{\bullet-}$ nanoprobe exhibited high sensitivity in the detection of $O_2^{\bullet-}$ at picomole level with prolonged CL time and prominent biocompatibility. In addition, coelenterazine was also found to be a sensitive reporter of intracellular $O_2^{\bullet-}$, and the function and mass of beta cells were monitored by $O_2^{\bullet-}$ imaging [85].

3.2. Inorganic material-based CL imaging

Although the POCL reactions have demonstrated highly sensitive and selective response in *in vivo* CL imaging, most reagents used in POCL were hydrophobic. Recently, a hydrophilic POCL silica nanodevice was developed for intracellular imaging of H_2O_2 that was generated by oxidase-catalyzed biomarkers and was further applied for high throughput screening of insulin sensitizers [86]. In this POCL system (**Figure 6A**), CPPO and fluorescent reporter rhodamine B (RhB) were doped into the mesoporous silica NPs. The electrostatically adsorbed oxidases on the surface can not only catalyze the generation of H_2O_2 but also protect CPPO from leakage. Glucose in HepG2 cells and other oxidase-catalyzed biomarkers, such as lactic acid, uric acid, and ethanol, were imaged accurately using this POCL silica nanodevice. Besides, by adsorbing glucose oxidase (GOx) onto the surface of silica NPs, insulin sensitizers were successfully identified.

In addition to nonenzymatic POCL systems, based on silicon matrix, dual-functional NPs containing both HRP and Firefly luciferase (FLuc) were synthesized for in situ sequential imaging of ATP and H_2O_2 *in vivo* and *in vitro* (**Figure 6B**) [87]. For the synthesis of HRP-SiO_2@FLuc NPs, HRP was the core with the hydrolysis of tetraethyl orthosilicate. The surface of the core was amino-modified by (3-aminopropyl) triethoxysilane, and then Fluc was conjugated to the surface as shell. In the presence of ATP, enzymatic reaction of Fluc-$_D$-luciferin was carried out and the CL signals were imaged immediately. Then, HRP-SiO_2 core was broken at pH 5.5 and H_2O_2 was imaged by adding luminol. Two sequential CL signals were continuously recorded and imaged by a CL imaging system. The proposed strategy using HRP-SiO_2@FLuc nanoprobes successfully achieved sequential and sensitive detection of ATP and H_2O_2 in serum and BALB/c nude mice.

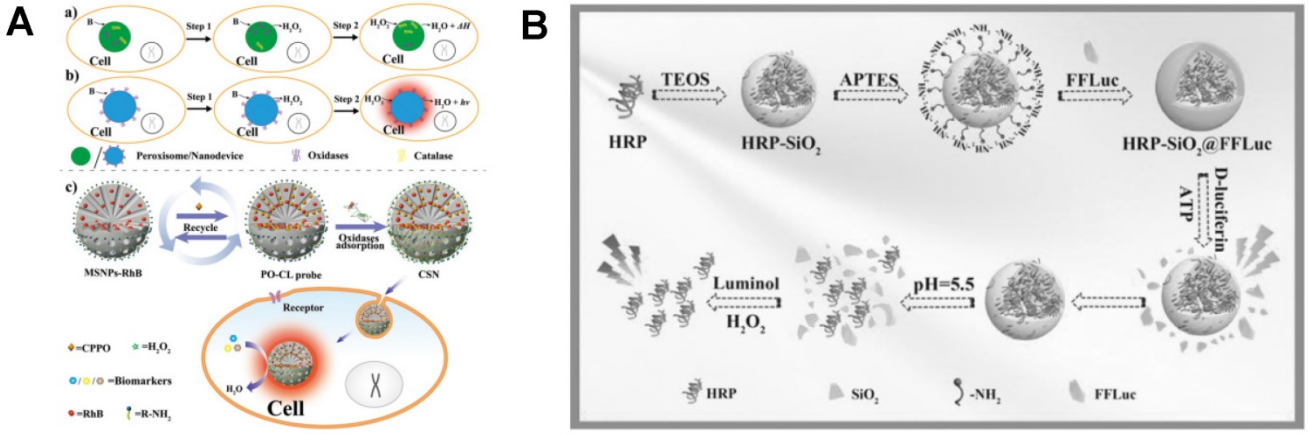

Figure 6. Silica NPs-based CL assays for *in vivo* H_2O_2 imaging. (A) Fabrication of POCL silica nanodevice for H_2O_2 imaging which was generated by different oxidase-catalyzed biomarkers. Reprinted with permission from [86], Copyright 2017, Wiley-VCH. **(B)** Synthesis of the HRP-SiO_2@FLuc NPs for in situ sequential imaging of endogenous and exogenous H_2O_2. Reprinted with permission from [87], Copyright 2016, Wiley-VCH.

Despite the increasing applications of organic dyes and polymer NPs, there are inherent limitations in CL imaging such as low light intensity. Alternatively, QDs with high quantum yield exhibit good stability against photobleaching. In order to reduce the cytotoxicity of QDs and increase their biocompatibility for *in vivo* imaging, polymer-covered and surface-modified QDs, poly(ethylene glycol)-QDs (PEG-QDs), were fabricated [88]. To detect *in vitro* and in *vivo* H_2O_2, PEG and luminol derivative L012 were modified on the surface of QDs. CRET occurred in the L012-H_2O_2 CL system and the energy transferred to acceptor PEG-QDs, leading to a NIR emission. The detection limit of 0.5 μM exhibited sufficient sensitivity of this hybrid NPs for the detection of abnormal increased H_2O_2 level in mice.

3.3. Dioxetane-based CL imaging

Multiple CL substrates containing 1,2-dioxetane unit have been used in *in vivo* CL imaging assays, such as 3-(2'-spiroadamantyl)-4-methoxy-4-(3''-phosphoryloxyphenyl)-1,2-dioxetane (AMPPD) [89] and disodium 2-chloro-5-(4-methoxyspiro{1,2-dioxetane-3,2'-(5'-chloro)tricyclo [3.3.1.1^{3,7}]decan}-1-4-yl)-1-phenyl phosphate (CDP-Star) [90]. In recent years, more and more novel 1,2-dioxetane-based CL probes have been synthesized [91]. For example, Sijbesma's group developed a series of novel polymer for the research of mechanoluminescences. In this method, bis(adamantyl)-1,2-dioxetane unit was incorporated in a polymer chain or network to serve as luminescent mechanophore. After the polymeric chain or the network was treated with sonication, dioxetane crosslinkers were fractured and visible bright-blue CL was generated. The mechanically activated CL can transfer to suitable acceptors for color changes. Using 1,2-dioxetane as probe, real-time imaging of CL in chain-scission events can sense deformations, stresses and damage in polymers with high sensitivity [92].

Tissue oxygenation is a crucial indicator of tumor microenvironment and hypoxia usually leads to an increase of nitroreductase (NTR) in tumor cells. To real-time monitor NTR *in vivo*, an oxygen-dependent reductive probe, hypoxia chemiluminescent probe **2** (HyCL-**2**), was synthesized using 1,2-dioxetane scaffold for sensitive NTR CL imaging [93]. As shown in **Figure 7A**, H1299 lung tumors were grown subcutaneously in mice first. Then, tumor oxygenation was adjusted to 21% and 100% oxygen respectively before CL imaging using HyCL-**2**. After injecting a solution of HyCL-**2** and Emerald II enhancer in both mice, higher CL emission was imaged in 21% oxygen, which indicated that HyCL-**2** provided increased signals under low oxygenation condition in tumors. Further, due to the high stability and reduced background, HyCL-**2** showed ~170-fold increase in CL intensity in comparison with other small molecule reductants. Except for the above Emerald-II enhancer, dioxetane-fluorophore conjugates were also found to be remarkable enhancers for *in vivo* CL imaging of enzyme. Shabat et al. fabricated three turn-on fluorophore-tethered dioxetane CL probes for β-galactosidase imaging (**Figure 7B**) [94]. The resulting phenolate emitted various colors which conformed the fluorophore ultimately. Under the physiological condition, energy-transfer from excited dye (fluorescein or quinone-cyanine) to peroxy-dioxetane bond amplified the CL signal significantly without an external enhancer. Using CL microscopy, *in vivo* imaging was recorded after subcutaneous and intraperitoneal injection of the synthesized probes. The overexpression of β-galactosidase in HEK293 cells was also imaged sensitively.

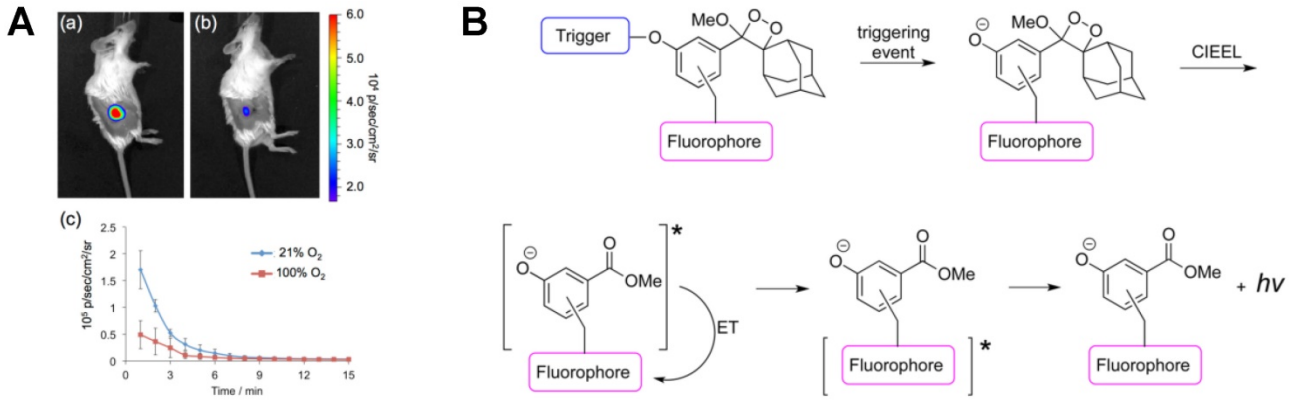

Figure 7. 1,2-dioxetane based CL probes for CL imaging. (A) *In vivo* imaging of H1299 lung tumor xenografts using HyCL-**2** under different oxygen concentrations. Reprinted with permission from [93], Copyright 2016, American Chemical Society. **(B)** CL mechanism of dioxetane-fluorophore conjugates. Reprinted with permission from [94], Copyright 2016, American Chemical Society.

Recently, to improve the thermal stability of the probes under physiological conditions, Shabat's group synthesized a series of thermostable dioxetane probes with enhanced CL emission in aqueous solution [95]. In consideration of the low quantum yield emission of excited state benzoate molecule released from Schaap's dioxetane, functionalization at the ortho-position of the phenol was adopted with highly enhanced CL emission. Different electron-withdrawing groups, such as acrylate and acrylonitrile, were installed on phenol donor [96]. The light emission intensity of the as-synthesized luminophore showed more than 3 orders of magnitude higher than that of the standard commercially available adamantylidene-dioxetane probe, achieving sensitive imaging of β-galactosidase and $^1O_2$ in cells [97]. Furthermore, through introducing dicyanomethylchromone to an extended π-electron system at the para-position of the phenol as acceptor, a luminophore with NIR emission was obtained with the maximum emission wavelength of 690 nm, which realized the CL imaging of both *in vitro* β-galactosidase and *in vivo* H_2O_2 [98]. In addition, elongated π-system and electron-withdrawing group were introduced to conventional Schaap's adamantylidene-dioxetane to increase the CL emission [99]. Then CGKRK peptide was conjugated on the luminophore using a maleimide as linker, which thus increased the aqueous solubility and cell permeability of luminophore under aqueous condition, realizing the first CL microscopy cell-imaging for cathepsin B detection. Besides, other novel luminophores such as CL formaldehyde probes [100], turn-on CL prodrug probes [101] and afterglow luminescent NPs with aggregation induced emission [102] were also synthesized for *in vivo* biosensing and cancer treatment.

4. BL imaging

Biological self-luminescence is a luminescence phenomenon produced by living organisms and the energy comes from enzymatic reactions rather than external light source [103]. Through sequencing and cloning, various luciferases were obtained from beetle and submarine luminescent animals for BL imaging [104, 105]. In *in vivo* BL imaging, luciferase is introduced into mammals or the luciferase gene is integrated into the cell chromosome, which then catalyzes the substrate luciferin to generate BL [106]. In BL process, no external light is required, and the efficiency from chemical energy to light energy is almost 100% [107]. Because of the high sensitivity, timeliness and good biocompatibility, BL imaging systems have now been widely applied to study tumor growth and metastasis [108], cell apoptosis and tracking [109], bacterial and virus infection [110], protein interactions and transgenes [111] in life sciences, medical researches and drug development. In addition, re-engineered luciferases and chemical modification of the substrates further expand the applications of BL imaging [112, 113]. Furthermore, some novel probes, such as upconversion NPs and QDs have been integrated with the traditional luciferase systems to improve the imaging sensitivity [114-116]. With the advances in imaging technologies, such as modular low-light microscope, BL imaging has become more and more popular [117-119]. In the previous reviews, the traditional luciferase-luciferin BL imaging systems have been systematically summarized [120-126]. Among them, D-luciferin-Fluc, D-luciferin-click beetle luciferase, *Renilla reniformis* luciferase (RLuc)-coelenterazine and *Gaussia princeps* luciferase (GLuc)-coelenterazine pairs have been applied in BL imaging of gene expression, protein interactions, enzyme activities and transplanted cells. In this review, we not only summarize the traditional

luciferase-luciferin reporters, but also demonstrate new luciferases and genetic engineering as well as novel BL substrates.

4.1. In situ formation of luciferase for BL imaging

Because of the good biocompatibility and high sensitivity, BL imaging has been applied to study the processes and pathways in neurological disorders, especially the brain-related inflammation and diseases [127]. Alzheimer is a neurodegenerative disease, which closely relates to the production and deposition of Aβ peptide [128]. Gfap-luciferase was used to monitor the accumulation of Aβ in transgenic mouse models by a rapid, noninvasive and quantitative BL imaging strategy [129]. Moreover, the effects of combretastatin-A4P on brain tumor xenografts were tracked in real time using dynamic BL imaging both in 9L rat glioma cells and living mice brain [130]. To improve the accuracy, in situ formation of luciferase was introduced to *in vivo* BL imaging, which can greatly reduce the imaging background. For example, the split-Fluc reporter system has been successfully applied to monitor the formation of α-synuclein (αSYN) oligomers through the release of Fluc after interaction between N-terminal (NFluc) and C-terminal (CFluc) part of Fluc, which demonstrated that the inhibitor FK506 can reduce the oligomerization of αSYN [131].

Sphingosine-1-phosphate receptor 1 ($S1P_1$) is one of the G protein-coupled receptors and is widely distributed in tissues, which plays an important role in both nervous and immune systems. Richard' group constructed a genetic model in U2OS cells, in which $S1P_1$ and β-arrestin2 were linked to CLuc and NLuc, respectively (**Figure 8**) [132]. The activation of $S1P_1$ promoted its interaction with β-arrestin2, leading to the association of inactive luciferase fragments and the production of an active enzyme complex $S1P_1$-CLuc/NLuc-β-arrestin2. In the presence of ATP and $_D$-luciferin, the BL images were recorded clearly. After the model was optimized, $S1P_1$ activation was used to monitor LPS caused inflammation in brain of mice via real-time BL imaging.

4.2. Luciferase mutants for BL imaging

The choice of luciferase is crucial in BL imaging. The commonly used luciferases, such as Fluc and GLuc, are often limited in the imaging of deep tissues and cell tracking. Even the emerging NanoLuc is still restricted by the emission of predominantly blue. Thus, the development of novel luciferase genes and mutants has been of great concern over the past decade. Transformed by genetic engineering and functional groups, novel luciferases are increasingly applied in BL systems. Among them, a thermostable red-shifted luciferase PpyRE9H (λ_{max} = 617 nm) was designed to study parasite infections in deep tissue [133]. In this work, the gene of PpyRE9H was mutated by 5'-variant surface glycoprotein and 3'-tubulin untranslated regions, which showed high sensitivity in BL imaging. Moreover, PLG2 luciferase was found to be a reliable substitute to luc2 gene for imaging ATP with enhanced thermal and pH stability combining with beetle luciferin [134]. To improve the selectivity of the substrate, Spencer et al. synthesized a series of luciferases with mutated active sites and aminoluciferin substrates (**Figure 9A**) [135]. It has been found that the strong BL signals can be imaged from the luciferase L342A that was produced by the mutation of leucine 342 using the aminoluciferin CycLuc2-amide, which achieved substrate selectivity as expected.

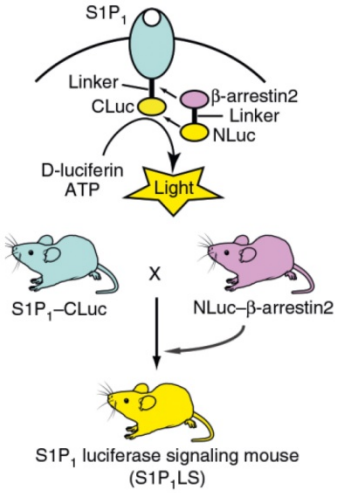

Figure 8. In situ formation of luciferase and the mating scheme of $S1P_1$ luciferase signaling mice. Reprinted with permission from [132], Copyright 2017, Nature Publishing Group.

The cell tracking and intercellular communicates have been systematically studied by BL imaging using a triple imaging system containing FLuc, GLuc and *Vargula hilgendorfii* luciferase [136]. At the same time, the oscillation kinetics and cellular mechanisms of cells were also well investigated [137, 138]. But multicomponent imaging of cells was also limited by the poor substrate selectivity of luciferases. To differentiate cell types, a family of orthogonal luciferase-luciferin pairs were produced through steric modification [107]. As shown in **Figure 9B**, residues 218, 249-251, and 314-316 were selected to mutagenesis. The mutated luciferase library was then incubated with sterically modified luciferins. Based on the proximity between luciferase and the C7', C4' of luciferins, functional mutants were screened out accurately, which was also used to study the orthogonality of other mutants and analogues.

Multiple orthogonal pairs with different light emission were screened out and successfully used for BL imaging of different cells, demonstrating that this library screening strategy provided a powerful method for exploring new BL probes. Very recently, Miyawaki et al. synthesized the Akaluc via the iterative screening of candidates with multiple cycles [109]. Using AkaLumine as substrate, the BL emission was significantly enhanced and both *in vitro* and *in vivo* imaging of tumorigenic cells were realized. Furthermore, the NIR emission of BL made it penetrated body walls easily, achieving BL imaging of single-cell in deep tissue of moving mice using AkaLumine-Akaluc pairs.

Dual-color imaging was also used to improve the sensitivity of BL imaging [139]. Mayu et al. used Emerald Luc and Stable Luciferase Red as reporters to track the subcellular localization and gene expressions simultaneously [140]. Dual-color system of red and green was also used for malaria research, which achieved single-cell imaging as well as the measurement of stage-specific drug effects on parasites [141]. The intestinal persistence of *lactobacillus plantarum* and *lactococcus lactis* was monitored through combination of CBRluc and CBGluc with dual-color BL imaging strategy [142]. Through combining beetle luciferin analogues and different engineered Fluc, Amit et al. developed a series of BL systems emitted from far red to NIR light [143].

4.3. In situ formation of luciferin for BL imaging

In situ release of luciferin was as effective as target-triggered luciferase formation. So far, a series of luciferin-based conjugates have been reported for *in vivo* BL imaging. A turn-on BL probe containing nitro group was designed for visualization of endogenous NTR in living cells and mice with high selectivity and selectivity (**Figure 10A**) [144]. In this study, D-luciferin-Fluc pair with different caged groups and linkers was used. After mixing BL probe with NTR and cofactor NADH, the selective reduction occurred and the nitro group in the probe transformed into amino group. Then cleavage reaction led to the release of free firefly luciferin to activate the catalytic reaction with luciferase and subsequently produced a photon. Even 0.001 μg/mL of NTR can be explicitly observed using this probe.

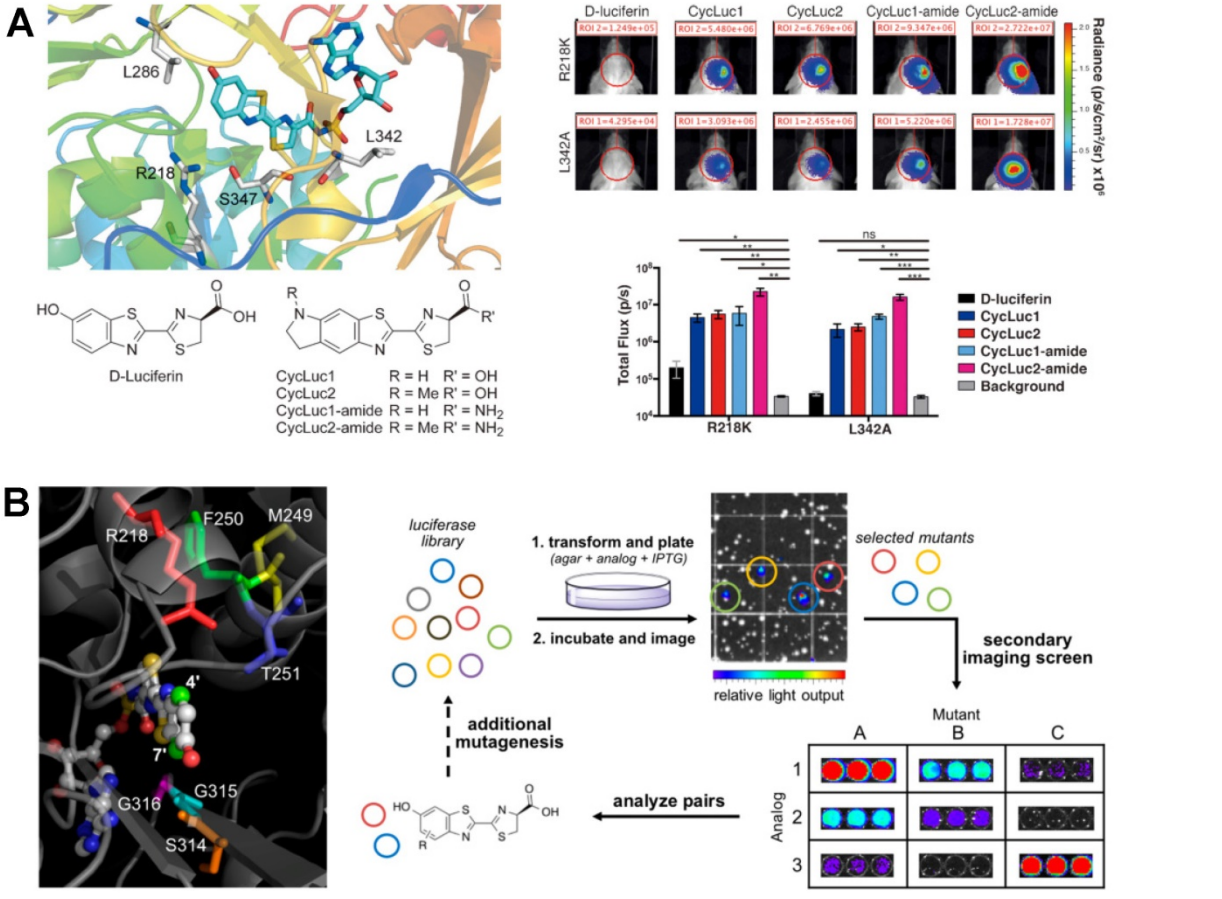

Figure 9. BL imaging with luciferase mutants. (A) Crystal structure of luciferase with different mutations, the structure of aminoluciferin analogues, and the performance of mutant luciferase with different luciferins in the brains of live mice. Reprinted with permission from [135], Copyright 2016, Wiley-VCH. **(B)** Amino acids targeted for mutagenesis and library screening strategy. Reprinted with permission from [107], Copyright 2017, American Chemical Society.

Luciferin-based BL imaging probes were also used to detect *in vivo* metal ions. For example, iron-caged luciferin-1 (ICL-1), an endoperoxide-luciferin conjugate, was synthesized for longitudinal monitoring of labile iron pools in living mice [145]. The presence of Fe^{2+} caused the cleavage of conjugate and the release of D-aminoluciferin, which generated an increased BL signal that was correlated with the amount of Fe^{2+}. Very recently, the accumulation of Co^{2+} was also imaged via the split of luciferin-based conjugate [146]. The Co^{2+} BL probe 1 (CBP-1) was synthesized using the N_3O ligand and a C-O benzyl ether bond, in which the tetradentate ligand N_3O was the trigger for Co^{2+}. As shown in **Figure 10B**, only in the presence of Co^{2+}, D-luciferin substrate was released due to the cleavage of Co^{2+}-mediated C-O bond in CBP-1, resulting in an increased BL intensity. Using the CBP-1, the accumulation and fluctuation of Co^{2+}, as well as ATP and luciferase, were sensitively monitored real-time in a mouse model.

Besides metal ions, CO in living cells and mice was also imaged using BL based on the Tsuji-Trost reaction of allyl-luciferin probe [147]. Non-luminous luciferin-based conjugate of allyl-luciferin was synthesized and used as a novel BL probe. After injecting allyl-luciferin and $PdCl_2$-containing liposomes intraperitoneally and intratumorally, $[Ru(CO)_3Cl$-(glycinate)] was then injected to produce exogenous CO. Subsequently, $PdCl_2$ was reduced to Pd^0 by CO and Pd^0-mediated Tsuji-Trost reaction led to the yield of D-luciferin, realizing the real-time BL imaging of CO. This turn-on probe demonstrated good sensitivity and selectivity to both exogenous and endogenous CO. Moreover, a silent BL probe acrylic ester luciferin was synthesized for Cys detection both *in vitro* and *in vivo* (**Figure 10C**) [148]. The BL probe was synthesized through caging hydroxyl group of D-luciferin motif by acrylic ester. In the presence of Cys, a conjugate addition of Cys to acrylate occurred, leading to the in situ release of D-luciferin for BL imaging. This BL probe could selectively detect Cys with a LOD of 88 nM *in vitro*, and Cys in living mice was also sensitively analyzed.

In addition to luciferin-based conjugates, in situ formation of luciferin via a pair of complementary precursors was also applied in BL imaging [149]. Based on the formation of luciferin by two complementary precursors, Genevieve et al. presented an AND-type logic gate to detect H_2O_2 and caspase 8 activity simultaneously [150]. As shown in **Figure 10D**, the probes of peroxy caged luciferin-2 (PCL-2) and z-Ile-Glu-ThrAsp-D-Cys were

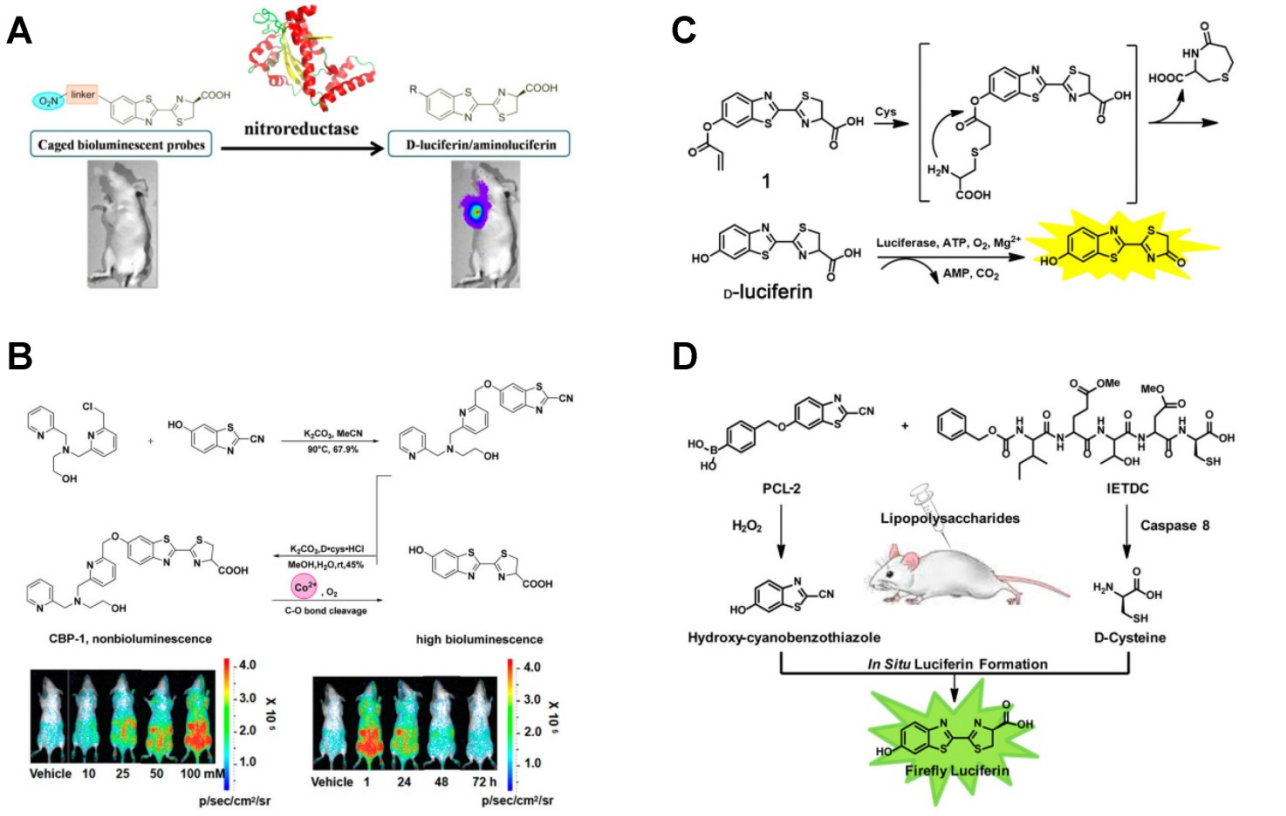

Figure 10. Luciferin-based conjugates as BL imaging probes. (A) *In vivo* release of firefly luciferin for endogenous NTR imaging. Reprinted with permission from [144], Copyright 2016, American Chemical Society. **(B)** Synthesis of CBP-1 and *in vivo* imaging of Co^{2+}. Reprinted with permission from [146], Copyright 2018, American Chemical Society. **(C)** Synthesis of acrylic ester luciferin and *in vivo* imaging of Cys. Reprinted with permission from [148], Copyright 2018, American Chemical Society. **(D)** Synchronous imaging of H_2O_2 and caspase 8 through in situ formation of luciferin. Reprinted with permission from [150], Copyright 2013, American Chemical Society.

synthesized with luciferin precursors respectively. After suffering from inflammation in mice (injection of LPS), the resulting H_2O_2 induced PCL-2 to produce 6-hydroxy-2-cyanobenzothiazole (HCBT) and the generated caspase 8 led to the release of D-cysteine via biochemical cleavage. The firefly luciferin was then in situ formed through a facile cyclization reaction between HCBT and D-cysteine, and the BL imaging was performed in the presence of Fluc for simultaneous detection of H_2O_2 and the activity of caspase 8. This method provided a powerful tool for concurrent monitoring and research of inflammation. In addition, caspase 3 was also sensitively imaged by N- and C-terminal fusion of the luciferin fragments [9, 151].

4.4. Luciferin analogs for BL imaging

D-luciferin is one of the most commonly used enzyme substrates to penetrate into cells, tissues and even whole organisms for imaging. Thus, simple and efficient synthesis of luciferin is of great importance to BL imaging. David et al. reported a rapid method to synthesize D-luciferin and a series of electronically modified nitrogenous analogues [152]. In the synthesis process, dithiazolium reagent was used to generate the heteroaromatic scaffolds in a divergent fashion. Two of the benzimidazole analogues with robust emission were found and applied in BL imaging in live cells. This synthesis method expanded the types of luciferin as well as the ability to rapidly access new luciferin substrates.

To satisfy the need of multicolor imaging, better biocompatibility and deep tissue penetration, the chemical modification of luciferin and the corresponding luciferin analogs came into being which emitted from the far-red to NIR ranges. The structures of D-luciferin as well as some D-luciferin-based analogs have been reported [153]. Retooling BL technology allowed the alteration of oxhydryl and sulfur atom of D-luciferin, therefore aminoluciferin, alkylaminoluciferin and other analogs were designed and applied to deep BL imaging *in vivo* [154, 155]. Further, a series of N-cyclo-alkylaminoluciferins and novel N-cyclobutylaminoluciferin were reported based on aminoluciferins [156].

Altering the 6′-position of D-luciferin via alkylation or acylation is an effective method to prepare luciferin analogs. To improve the sensitivity of *in vivo* BL imaging, Melanie et al. synthesized a new luciferin analog cyclic alkylaminoluciferin (CycLuc1) (**Figure 11A**) [157]. Through combing with the existing Fluc, CycLuc1 showed higher luminescence intensity, better light persistence and less dosage than D-luciferin, which was used to sensitively image 4T1 breast cancer cells and living mice. Although CycLuc1 as a novel luciferin has higher sensitivity than D-luciferin, its emission intensity (λ_{max} = 604 nm) in deep tissues is still weak or even unobservable. To achieve stronger penetration and lower tissue absorption, Takahiro et al. demonstrated a new luciferin analogue AkaLumine-HCl (Aka-HCl), which had the NIR emission (λ_{max} = 677 nm) and a significantly improved sensitivity in deep tissues (**Figure 11B**) [158]. The penetration efficiency of Aka-HCl was 5- and 8.3-fold higher than D-luciferin and 3.7- and 6.7-fold higher than CycLuc1 in 4- or 8-mm-thick tissue sections, respectively, presenting great potential in the detection of preclinical cancers. Similarly, based on the previous BL luciferin derivative 5′-fluoro and other small substituents [159], Rachel et al. successfully synthesized the D-luciferin-based 5′-alkyne derivative using C-H activation methodology [160]. The emission of alkynyl luciferin was comparatively red-shifted and its spectrum was similar to aminoluciferin. Meanwhile, this alkynyl luciferin was found to have good cell permeability after incubation with HEK293 cells.

Another challenge of luciferin in BL imaging is the durability of light emission. Only a long-time and real-time imaging *in vivo* or intracellular can reveal the intricate molecular dynamics. For example, the overexpression of fatty acid amide hydrolase (FAAH) is closely related to the nervous system diseases. However, current BL imaging of FAAH can only last 5 h [161]. To better explain the nosogenesis of FAAH, Yue et al. designed a D-luciferin-based BL probe (D-Cys-Lys-CBT)$_2$ for intracellular BL imaging [162]. As shown in **Figure 11C**, after (D-Cys-Lys-CBT)$_2$ entered the cells via endocytosis, intracellular reduction reaction was triggered by GSH to form cyclic D-luciferin NPs. Cycloaddition promoted the formation of (D-Cys-Lys-CBT)$_2$-dimer, and (D-Cys-Lys-CBT)$_2$ NPs were finally formed through the self-assembly of dimers. Before hydrolysis, (D-Cys-Lys-CBT)$_2$ NPs lurked steadily inside the cells until the emergence of FAAH. FAAH-induced hydrolysis caused the slow release of D-luciferin or its derivatives, which ensured the persistance of BL as well as the long-time tracking of FAAH *in vivo*. It was found that the BL intensity in tumors of mice injected with (D-Cys-Lys-CBT)$_2$ reached its peak at 24 h and sustained an imageable signal for at least 2.5 days, which was markedly longer than aminoluciferin methyl amide, Lys-amino-D-luciferin and amino-D-luciferin.

4.5 BRET imaging

Through introduction of acceptor chromophore to BL system, the luminescence generated from

luciferase would be transferred to the acceptor chromophore through BRET. In this way, the luminous intensity and the maximum emission of luciferase changed, which displayed significant effect on the sensitivity of BL imaging [163]. The signal of BRET is a ratio rather than an absolute quantity, so it could eliminate the data variables that result from cell numbers, cell types, and other experimental variables. Because of the red-shifts of maximum emission, BRET has been increasingly applied to investigate protein interactions and intracellular molecular dynamics [164]. For example, Xiong et al. synthesized a self-luminescing BRET-FRET polymer nanoprobe with strong NIR emission for lymph-node mapping and tumor imaging to avoid the short-wavelength autofluorescence *in vivo* [165]. Through combining BRET and improved light intensity, Jun et al. reported a fluorescent protein CyOFP1 through engineering the orange-red fluorescent proteins [166]. The red-emitting Antares (the fusion of CyOFP1 and NanoLuc) was synthesized using NanoLuc as the donor and CyOFP1 as the acceptor to facilitate the BRET. In comparison with Fluc and other BL proteins, this BL reporter generated greatly brighter signals in deep tissues. Very recently, Yeh et al. successfully synthesized and screened out the analogues of coelenterazine, diphenylterazine (DTZ) and selenoterazine (STZ) (**Figure 12**) [167]. One mutant of NanoLuc NanoLuc-D19S/D85N/C164H, designated as 'teLuc', was found to enhance the emission of DTZ with 5.7-fold. The NanoLuc in Antares was replaced with teLuc, and the BRET-based Antares2 reporter was formed. The Antares2-DTZ pairs showed obvious red-shifted emission in comparison with Antares and FLuc-D-luciferin, which also demonstrated excellent tissue penetration efficiency in living mice imaging.

In addition to imaging, BRET has also been applied in PDT. Yuan et al. used cationic oligo(p-phenylene vinylene) (OPV) to absorb the CL of luminol and then produce ROS through BRET to kill the adjacent cancer cells and pathogenic microbes *in vivo* [168]. Unlike the other PDT strategies, this molecule-induced system used OPV as the photosensitizer, which didn't require an external light source.

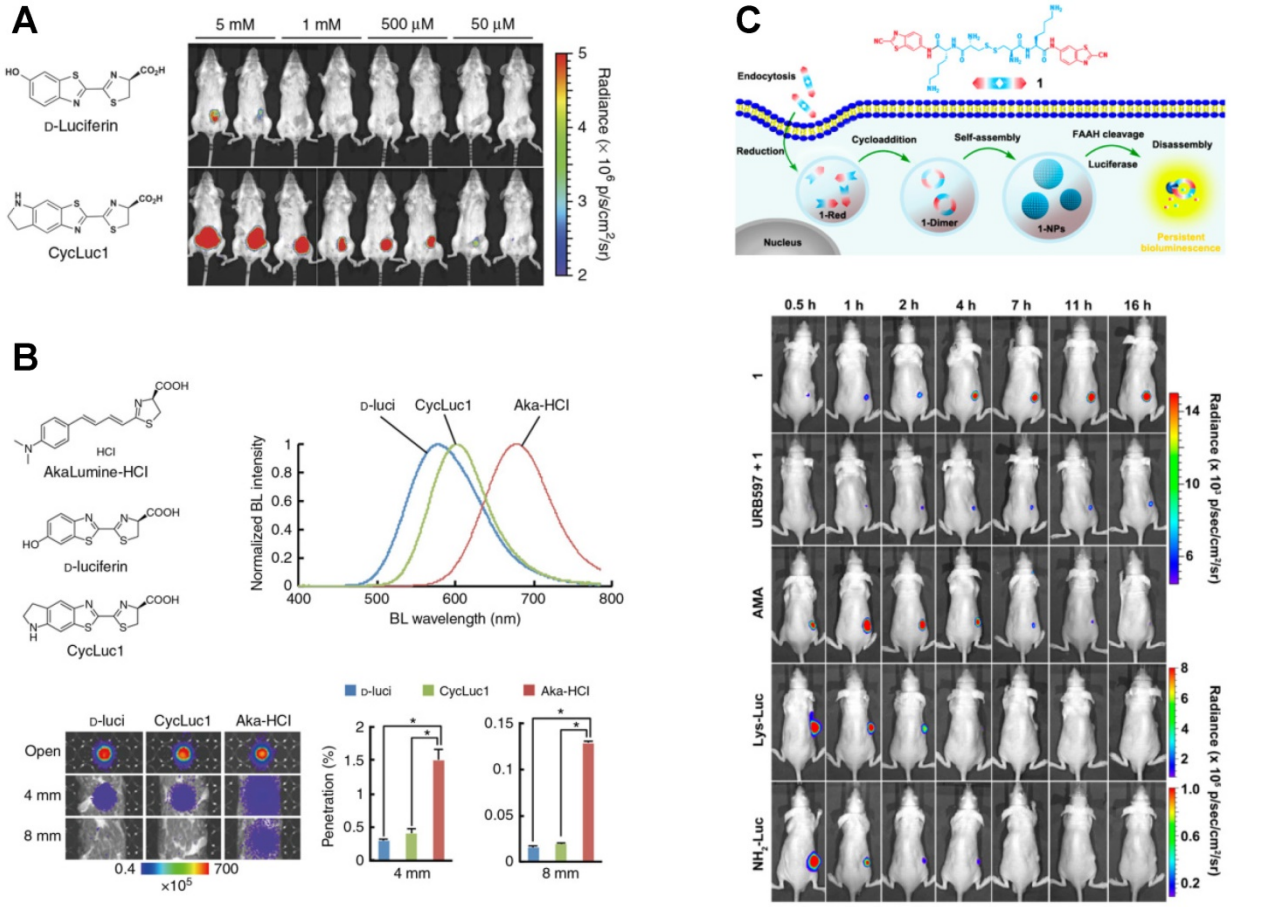

Figure 11. Luciferin analogs for BL imaging. (A) Structures and imaging sensitivity of CycLuc1 compared to D-luciferin. Reprinted with permission from [157], Copyright 2014, Nature Publishing Group. **(B)** Structures, BL emission spectra and tissue penetration efficiency of AkaLumine-HCl, CycLuc1 and D-luciferin. n = 3, *P < 0.05 (*t*-test). Reprinted with permission from [158], Copyright 2016, Nature Publishing Group. **(C)** Long-term BL imaging of FAAH using (D-Cys-Lys-CBT)2. Reprinted with permission from [162], Copyright 2016, American Chemical Society.

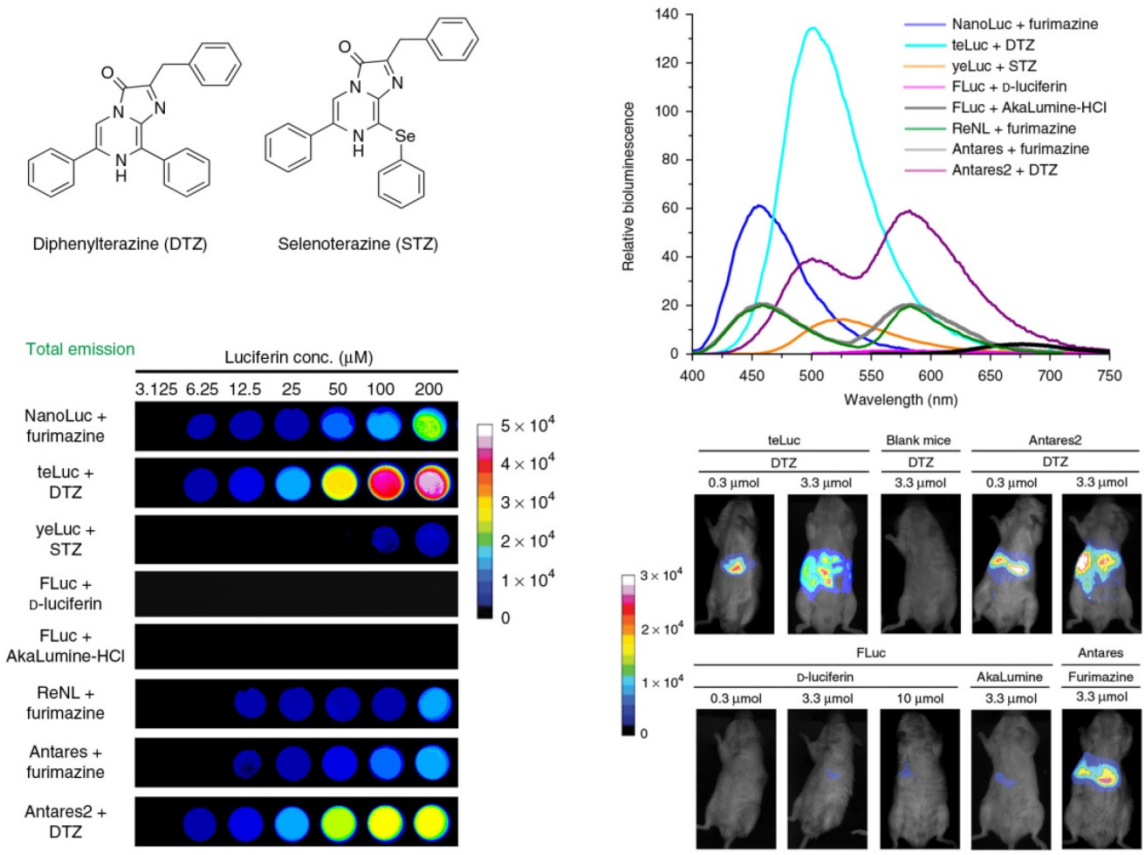

Figure 12. Chemical structures and BL emission of the synthetic luciferins (DTZ and STZ) as well as their corresponding BL imaging in HEK 293T cells and live mice in the presence of various re-engineered luciferases. Reprinted with permission from [167], Copyright 2017, Nature Publishing Group.

5. Conclusions and perspectives

CL and BL imaging have attracted great interest because of their high SNR, wide linear dynamic range and real-time performance. In the field of chemistry and biology, both of them and their derived methods provide powerful tools for *in vitro* and *in vivo* detection of a wide range of analytes. With the emergence of new luminescent materials and systems, as well as the combination with other technologies such as ELISA and molecularly imprinted polymer, the sensitivity and selectivity of CL and BL imaging methods have been significantly improved.

However, there are still some challenges in CL and BL imaging. Firstly, most CL systems are quick and the light emission is completed within seconds so that the data acquisition and imaging is relatively difficult. To overcome this defect, slow CL reactions, such as POCL systems have been reported [36]. It is necessary to explore new luminescent agents for reducing the delay between reaction and signal acquisition. Recently, persistent luminescence with long time emission has become a new optical imaging modality, which can avoid autofluorescence and background. So far, more and more persistent luminescence nanoprobes have been explored for bioimaging and therapeutic applications [169, 170]. Another challenge is the high requirement of instruments. CCD cameras are often limited in microarrays, microplates and high throughput reactions to capture the light signal. Therefore, the development of camera equipment with high resolution, high sensitivity and anti-interference ability is necessary in further applications of CL and BL imaging. In addition, for *in vivo* applications, the absorption of tissues, weak light intensity and multicomponent analysis put forward higher requirements for CL and BL imaging technologies. It is confident that CL and BL imaging will become powerful techniques in the fields of biochemical analysis, clinical diagnosis and treatment of diseases, environmental monitoring, and so on.

Abbreviations

αSYN: α-synuclein; μCADs: microfluidic cloth-based analytical devices; Aka-HCl: AkaLumine-HCl; AMPPD: 3-(2′-spiroadamantyl)-4-methoxy-4-(3″-phosphoryloxyphenyl)-1,2-dioxetane; AuNPs: gold nanoparticles; BL: bioluminescence; BLSA: 9,10-distyrylanthracene derivative; BRET: bioluminescence resonance energy transfer; CBP-1: Co^{2+} BL probe 1; CCD: charge-coupled device;

CDP-Star: disodium 2-chloro-5-(4-methoxyspiro{1,2-dioxetane-3,2'-(5'-chloro)tricyclo [3.3.1.1^{3,7}]decan}-1-4-yl)-1-phenyl phosphate; CF-polymer NPs: CRET-FRET-polymer NPs; CL: chemiluminescence; CPPO: bis[3,4,6-trichloro-2-(pentyloxycarbonyl)phenyl] oxalate; CPs: conjugated polymers; CRET: chemiluminescence resonance energy transfer; Cy5: 3,3'-diethylthiadicarbocyanine iodide; CycLuc1: cyclic alkylaminoluciferin; Cys: cysteine; DTZ: diphenylterazine; ECL: electrogenerated chemiluminescence; FAAH: fatty acid amide hydrolase; Fluc: Firefly luciferase; GLuc: *Gaussia princeps* luciferase; GO: graphene oxide; GOx: glucose oxidase; HCBT: 6-hydroxy-2-cyanobenzothiazole; HPOX: hydroxylbenzyl alcohol-incorporated copolyoxalate; HRP: horseradish peroxidase; HyCL-**2:** hypoxia chemiluminescent probe **2**; ICL-1: iron-caged luciferin-1; iNAAT: isothermal nucleic acid amplification test; LPS: lipopolysaccharide; NGQDs: nitrogen-doped graphene quantum dots; NIR: near-infrared; NPs: nanoparticles; NTR: nitroreductase; OPV: oligo(p-phenylene vinylene); PCL-2: peroxy caged luciferin-2; PCLA: polycaprolactone monoacrylate; PCR: polymerase chain reaction; PDT: photodynamic therapy; PEG-QDs: poly(ethylene glycol)-QDs; POCL: peroxyoxalate chemiluminescence; PPV: poly(phenylenevinylene); PTT: photothermal therapy; QDs: quantum dots; RhB: rhodamine B; RLuc: *Renilla reniformis* luciferase; RPA: recombinase polymerase amplification; S1P$_1$: sphingosine-1-phosphate receptor 1; SCLM: scanning CL microscopy; SECM: scanning electrochemical microscopy; SNR: signal-noise ratio; STZ: selenoterazine; TBD: TPE-BT-DC; TCPO: bis(2,4,6-trichlorophenyl) oxalate.

Acknowledgements

This work was supported by the National Natural Science Foundation of China (21722505, 21535002 and 21705086), the Special Funds of the Taishan Scholar Program of Shandong Province (tsqn20161028), and the Natural Science Foundation of Shandong Province (ZR2017JL009), and the Foundation of Key Laboratory of Sensor Analysis of Tumor Marker, Ministry of Education, Qingdao University of Science and Technology (SATM201803).

Competing Interests

The authors have declared that no competing interest exists.

References

1. Aboul-Enein HY, Stefan R-I, van Staden JF, Zhang XR, Garcia-Campana AM, Baeyens WRG. Recent developments and applications of chemiluminescence sensors. Crit Rev Anal Chem. 2000; 30: 271-89.
2. Roda A, Guardigli M, Pasini P, Mirasoli M, Michelini E, Musiani M. Bio- and chemiluminescence imaging in analytical chemistry. Anal Chim Acta. 2005; 541: 25-36.
3. Jansen EHJM, Buskens CAF, van den Berg RH. A sensitive CCD image system for detection of chemiluminescent reactions. J Biolumin Chemilumin. 1989; 3: 53-7.
4. Créton R, Jaffe LF. Chemiluminescence microscopy as a tool in biomedical research. Biotechniques. 2001; 31: 1098-100.
5. Momeni N, Ramanathan K, Larsson PO, Danielsson B, Bengmark S, Khayyami M. CCD-camera based capillary chemiluminescent detection of retinol binding protein. Anal Chim Acta. 1999; 387: 21-7.
6. Yang M, Kostov Y, Bruck HA, Rasooly A. Carbon nanotubes with enhanced chemiluminescence Immunoassay for CCD-based detection of staphylococcal enterotoxin B in food. Anal Chem. 2008; 80: 8532-7.
7. Suzuki K, Nagai T. Recent progress in expanding the chemiluminescent toolbox for bioimaging. Curr Opin Biotechnol. 2017; 48: 135-41.
8. Hananya N, Shabat D. A glowing trajectory between bio- and chemiluminescence: from luciferin-based probes to triggerable dioxetanes. Angew Chem Int Ed. 2017; 56: 16454-63.
9. Niu G, Zhu L, Ho DN, Zhang F, Gao H, Quan Q, et al. Longitudinal bioluminescence imaging of the dynamics of Doxorubicin induced apoptosis. Theranostics. 2013; 3: 190-200.
10. Lim C-K, Lee Y-D, Na J, Oh JM, Her S, Kim K, et al. Chemiluminescence-generating nanoreactor formulation for near-infrared imaging of hydrogen peroxide and glucose level in vivo. Adv Funct Mater. 2010; 20: 2644-8.
11. Pu KY, Chattopadhyay N, Rao JH. Recent advances of semiconducting polymer nanoparticles in in vivo molecular imaging. J Control Release. 2016; 240: 312-22.
12. Kaskova ZM, Tsarkova AS, Yampolsky IV. 1001 lights: luciferins, luciferases, their mechanisms of action and applications in chemical analysis, biology and medicine. Chem Soc Rev. 2016; 45: 6048-77.
13. England CG, Ehlerding EB, Cai W. NanoLuc: A small luciferase is brightening up the field of bioluminescence. Bioconjugate Chem. 2016; 27: 1175-87.
14. de Almeida PE, van Rappard JRM, Wu JC. In vivo bioluminescence for tracking cell fate and function. Am J Physiol Heart Circ Physiol . 2011; 301: H663-H71.
15. Yao Z, Zhang BS, Prescher JA. Advances in bioluminescence imaging: new probes from old recipes. Curr Opin Chem Biol. 2018; 45: 148-56.
16. Dodeigne C, Thunus L, Lejeune R. Chemiluminescence as a diagnostic tool. A review. Talanta. 2000; 51: 415-39.
17. Li J, Rao J, Pu K. Recent progress on semiconducting polymer nanoparticles for molecular imaging and cancer phototherapy. Biomaterials. 2018; 155: 217-35.
18. Luo L, Zhang Z, Ma L. Determination of recombinant human tumor necrosis factor-α in serum by chemiluminescence imaging. Anal Chim Acta. 2005; 539: 277-82.
19. Chouhan RS, Vivek Babu K, Kumar MA, Neeta NS, Thakur MS, Amitha Rani BE, et al. Detection of methyl parathion using immuno-chemiluminescence based image analysis using charge coupled device. Biosens Bioelectron. 2006; 21: 1264-71.
20. Bi S, Zhou H, Zhang S. Multilayers enzyme-coated carbon nanotubes as biolabel for ultrasensitive chemiluminescence immunoassay of cancer biomarker. Biosens Bioelectron. 2009; 24: 2961-6.
21. Jans H, Huo Q. Gold nanoparticle-enabled biological and chemical detection and analysis. Chem Soc Rev. 2012; 41: 2849-66.
22. Hutter E, Maysinger D. Gold-nanoparticle-based biosensors for detection of enzyme activity. Trends Pharmacol Sci. 2013; 34: 497-507.
23. Bi S, Yan Y, Yang X, Zhang S. Gold nanolabels for new enhanced chemiluminescence immunoassay of Alpha-fetoprotein based on magnetic beads. Chem--Eur J. 2009; 15: 4704-9.
24. Zong C, Wu J, Wang C, Ju H, Yan F. Chemiluminescence imaging immunoassay of multiple tumor markers for cancer screening. Anal Chem. 2012; 84: 2410-5.
25. Zong C, Wu J, Xu J, Ju H, Yan F. Multilayer hemin/G-quadruplex wrapped gold nanoparticles as tag for ultrasensitive multiplex immunoassay by chemiluminescence imaging. Biosens Bioelectron. 2013; 43: 372-8.
26. Chen Y, Sun J, Xianyu Y, Yin B, Niu Y, Wang S, et al. A dual-readout chemiluminescent-gold lateral flow test for multiplex and ultrasensitive detection of disease biomarkers in real samples. Nanoscale. 2016; 8: 15205-12.
27. Pang J, Zhao Y, Liu H-L, Wang K. A single nanoparticle-based real-time monitoring of biocatalytic progress and detection of hydrogen peroxide. Talanta. 2018; 185: 581-5.
28. Han E, Ding L, Qian R, Bao L, Ju H. Sensitive chemiluminescent imaging for chemoselective analysis of glycan expression on living cells using a multifunctional nanoprobe. Anal Chem. 2012; 84: 1452-8.
29. Gao Y, Li B. Exonuclease III-assisted cascade signal amplification strategy for label-free and ultrasensitive chemiluminescence detection of DNA. Anal Chem. 2014; 86: 8881-7.
30. Gao Y, Li B. G-quadruplex DNAzyme-based chemiluminescence biosensing strategy for ultrasensitive DNA detection: combination of exonuclease III-assisted signal amplification and carbon nanotubes-assisted background reducing. Anal Chem. 2013; 85: 11494-500.

31. Bi S, Zhou H, Zhang S. Bio-bar-code functionalized magnetic nanoparticle label for ultrasensitive flow injection chemiluminescence detection of DNA hybridization. Chem Commun. 2009: 5567-9.
32. Bi S, Hao S, Li L, Zhang S. Bio-bar-code dendrimer-like DNA as signal amplifier for cancerous cells assay using ruthenium nanoparticle-based ultrasensitive chemiluminescence detection. Chem Commun. 2010; 46: 6093-5.
33. Bi S, Zhou H, Zhang S. A novel synergistic enhanced chemiluminescence achieved by a multiplex nanoprobe for biological applications combined with dual-amplification of magnetic nanoparticles. Chem Sci. 2010; 1: 681-7.
34. Nam J-M, Thaxton CS, Mirkin CA. Nanoparticle-based bio-bar codes for the ultrasensitive detection of proteins. Science. 2003; 301: 1884-6.
35. Bi S, Ji B, Zhang Z, Zhang S. A chemiluminescence imaging array for the detection of cancer cells by dual-aptamer recognition and bio-bar-code nanoprobe-based rolling circle amplification. Chem Commun. 2013; 49: 3452-4.
36. Chen H, Wang Q, Shen Q, Liu X, Li W, Nie Z, et al. Nitrogen doped graphene quantum dots based long-persistent chemiluminescence system for ascorbic acid imaging. Biosens Bioelectron. 2017; 91: 878-84.
37. Vlatakis G, Andersson LI, Muller R, Mosbach K. Drug assay using antibody mimics made by molecular imprinting. Nature. 1993; 361: 645-7.
38. Haupt K, Mosbach K. Molecularly imprinted polymers and their use in biomimetic sensors. Chem Rev. 2000; 100: 2495-504.
39. Wulff G. Enzyme-like catalysis by molecularly imprinted polymers. Chem Rev. 2002; 102: 1-27.
40. Surugiu I, Danielsson B, Ye L, Mosbach K, Haupt K. Chemiluminescence imaging ELISA using an imprinted polymer as the recognition element instead of an antibody. Anal Chem. 2001; 73: 487-91.
41. Wang L, Zhang Z. Molecular imprinted polymer-based chemiluminescence imaging sensor for the detection of trans-resveratrol. Anal Chim Acta. 2007; 592: 115-20.
42. Wang L, Zhang Z. Chemiluminescence imaging assay dipyridamole based on molecular imprinted polymer as recognition material. Sens Actuators, B. 2008; 133: 40-5.
43. Wang L, Zhang Z, Huang L. Molecularly imprinted polymer based on chemiluminescence imaging for the chiral recognition of dansyl-phenylalanine. Anal Bioanal Chem. 2008; 390: 1431-6.
44. Zhang Y, Pang L, Ma C, Tu Q, Zhang R, Saeed E, et al. Small molecule-initiated light-activated semiconducting polymer dots: an integrated nanoplatform for targeted photodynamic therapy and imaging of cancer cells. Anal Chem. 2014; 86: 3092-9.
45. Liu F, Zhang C. A novel paper-based microfluidic enhanced chemiluminescence biosensor for facile, reliable and highly-sensitive gene detection of Listeria monocytogenes. Sens Actuators, B. 2015; 209: 399-406.
46. Zhang Y, Liu Q, Zhou B, Wang X, Chen S, Wang S. Ultra-sensitive chemiluminescence imaging DNA hybridization method in the detection of mosquito-borne viruses and parasites. Parasit Vectors. 2017; 10.
47. Zhang Y, Liu Q, Wang D, Chen S, Wang X, Wang S. Genotyping and detection of common avian and human origin-influenza viruses using a portable chemiluminescence imaging microarray. SpringerPlus. 2016; 5: 1871.
48. Wang C, Xiao R, Dong P, Wu X, Rong Z, Xin L, et al. Ultra-sensitive, high-throughput detection of infectious diarrheal diseases by portable chemiluminescence imaging. Biosens Bioelectron. 2014; 57: 36-40.
49. Donhauser SC, Niessner R, Seidel M. Sensitive quantification of escherichia coli O157:H7, salmonella enterica, and campylobacter jejuni by combining stopped polymerase chain reaction with chemiluminescence flow-through DNA microarray analysis. Anal Chem. 2011; 83: 3153-60.
50. Bi S, Zhang Z, Dong Y, Wang Z. Chemiluminescence resonance energy transfer imaging on magnetic particles for single-nucleotide polymorphism detection based on ligation chain reaction. Biosens Bioelectron. 2015; 65: 139-44.
51. Yan Y, Yue S, Zhao T, Luo B, Bi S. Exonuclease-assisted target recycling amplification for label-free chemiluminescence assay and molecular logic operations. Chem Commun. 2017; 53: 12201-4.
52. Kunze A, Dilcher M, Abd El Wahed A, Hufert F, Niessner R, Seidel M. On-chip isothermal nucleic acid amplification on flow-Based chemiluminescence microarray analysis platform for the detection of viruses and bacteria. Anal Chem. 2015; 88: 898-905.
53. Xu Y, Li D, Cheng W, Hu R, Sang Y, Yin Y, et al. Chemiluminescence imaging for microRNA detection based on cascade exponential isothermal amplification machinery. Anal Chim Acta. 2016; 936: 229-35.
54. Bi S, Xiu B, Ye J, Dong Y. Target-catalyzed DNA four-way junctions for CRET Imaging of microRNA, concatenated logic operations, and self-assembly of DNA nanohydrogels for targeted drug delivery. ACS Appl Mater Interfaces. 2015; 7: 23310-9.
55. Xu Y, Luo J, Wu M, Hu F, Lu Z, Jing H, et al. Ultrasensitive and specific imaging of circulating microRNA based on split probe, exponential amplification, and topological guanine nanowires. Sens Actuators, B. 2018; 269: 158-63.
56. Xu Y, Bian X, Sang Y, Li Y, Li D, Cheng W, et al. Bis-three-way junction nanostructure and DNA machineries for ultrasensitive and specific detection of BCR/ABL fusion gene by chemiluminescence imaging. Sci Rep. 2016; 6: 32370.
57. Yue S, Zhao T, Bi S, Zhang Z. Programmable strand displacement-based magnetic separation for simultaneous amplified detection of multiplex microRNAs by chemiluminescence imaging array. Biosens Bioelectron. 2017; 98: 234-9.
58. Guan W, Zhang C, Liu F, Liu M. Chemiluminescence detection for microfluidic cloth-based analytical devices (μCADs). Biosens Bioelectron. 2015; 72: 114-20.
59. Li H, Liu C, Wang D, Zhang C. Chemiluminescence cloth-based glucose test sensors (CCGTSs): a new class of chemiluminescence glucose sensors. Biosens Bioelectron. 2017; 91: 268-75.
60. Roda A, Mirasoli M, Dolci LS, Buragina A, Bonvicini F, Simoni P, et al. Portable device based on chemiluminescence lensless imaging for personalized diagnostics through multiplex bioanalysis. Anal Chem. 2011; 83: 3178-85.
61. Zangheri M, Di Nardo F, Mirasoli M, Anfossi L, Nascetti A, Caputo D, et al. Chemiluminescence lateral flow immunoassay cartridge with integrated amorphous silicon photosensors array for human serum albumin detection in urine samples. Anal Bioanal Chem. 2016; 408: 8869-79.
62. Tang CK, Vaze A, Rusling JF. Automated 3D-printed unibody immunoarray for chemiluminescence detection of cancer biomarker proteins. Lab Chip. 2017; 17: 484-9.
63. Michels DA, Tu AW, McElroy W, Voehringer D, Salas-Solano O. Charge heterogeneity of monoclonal antibodies by multiplexed imaged capillary isoelectric focusing immunoassay with chemiluminescence detection. Anal Chem. 2012; 84: 5380-6.
64. Delaney JL, Hogan CF, Tian J, Shen W. Electrogenerated chemiluminescence detection in paper-based microfluidic sensors. Anal Chem. 2011; 83: 1300-6.
65. Zhou H, Kasai S, Matsue T. Imaging localized horseradish peroxidase on a glass surface with scanning electrochemical/ chemiluminescence microscopy. Anal Biochem. 2001; 290: 83-8.
66. Hirano Y, Mitsumori Y, Oyamatsu D, Nishizawa M, Matsue T. Imaging of immobilized enzyme spots by scanning chemiluminescence microscopy with electrophoretic injection. Biosens Bioelectron. 2003; 18: 587-90.
67. Zhai Y, Zhu Z, Zhou S, Zhu C, Dong S. Recent advances in spectroelectrochemistry. Nanoscale. 2018; 10: 3089-111.
68. Lei R, Stratmann L, Schäfer D, Erichsen T, Neugebauer S, Li N, et al. Imaging biocatalytic activity of enzyme−polymer spots by means of combined scanning electrochemical microscopy/electrogenerated chemiluminescence. Anal Chem. 2009; 81: 5070-4.
69. Zhu B, Tang W, Ren Y, Duan X. Chemiluminescence of conjugated-polymer nanoparticles by direct oxidation with hypochlorite. Anal Chem. 2018; 90: 13714-22.
70. Liu M, Wu J, Yang K, Zong C, Lei J, Ju H. Proximity hybridization-regulated chemiluminescence resonance energy transfer for homogeneous immunoassay. Talanta. 2016; 154: 455-60.
71. Freeman R, Girsh J, Fang-ju Jou A, Ho J-aA, Hug T, Dernedde J, et al. Optical aptasensors for the analysis of the vascular endothelial growth factor (VEGF). Anal Chem. 2012; 84: 6192-8.
72. Zheng X, Qiao W, Wang ZY. Broad-spectrum chemiluminescence covering a 400–1400 nm spectral region and its use as a white-near infrared light source for imaging. RSC Adv. 2015; 5: 100736-42.
73. Liu Y, Han S. A chemiluminescence resonance energy transfer for the determination of indolyl acetic acid using luminescent nitrogen-doped carbon dots as acceptors. New J Chem. 2018; 42: 388-94.
74. Yao J, Li L, Li P, Yang M. Quantum dots: from fluorescence to chemiluminescence, bioluminescence, electrochemiluminescence, and electrochemistry. Nanoscale. 2017; 9: 13364-83.
75. Yue S, Zhao T, Qi H, Yan Y, Bi S. Cross-catalytic hairpin assembly-based exponential signal amplification for CRET assay with low background noise. Biosens Bioelectron. 2017; 94: 671-6.
76. Yan L, Pu K. Recent advances of activatable molecular probes based on semiconducting polymer nanoparticles in sensing and imaging. Adv Sci. 2017; 4: 1600481.
77. Lee D, Khaja S, Velasquez-Castano JC, Dasari M, Sun C, Petros J, et al. In vivo imaging of hydrogen peroxide with chemiluminescent nanoparticles. Nat Mater. 2007; 6: 765-9.
78. Lee YD, Lim CK, Singh A, Koh J, Kim J, Kwon IC, et al. Dye/peroxalate aggregated nanoparticles with enhanced and tunable chemiluminescence for biomedical imaging of hydrogen peroxide. Acs Nano. 2012; 6: 6759-66.
79. Cho S, Hwang O, Lee I, Lee G, Yoo D, Khang G, et al. Chemiluminescent and antioxidant micelles as theranostic agents for hydrogen peroxide associated-inflammatory diseases. Adv Funct Mater. 2012; 22: 4038-43.
80. Mao D, Wu W, Ji S, Chen C, Hu F, Kong D, et al. Chemiluminescence-guided cancer therapy using a chemiexcited photosensitizer. Chem. 2017; 3: 991-1007.
81. Shuhendler AJ, Pu K, Cui L, Uetrecht JP, Rao J. Real-time imaging of oxidative and nitrosative stress in the liver of live animals for drug-toxicity testing. Nat Biotechnol. 2014; 32: 373-80.
82. Zhen X, Zhang C, Xie C, Miao Q, Lim KL, Pu K. Intraparticle energy level alignment of semiconducting polymer nanoparticles to amplify chemiluminescence for ultrasensitive in vivo imaging of reactive oxygen species. ACS Nano. 2016; 10: 6400-9.
83. Zhen X, Xie C, Pu KY. Temperature-correlated afterglow of a semiconducting polymer nanococktail for imaging-guided photothermal therapy. Angew Chem Int Ed Engl. 2018; 57: 3938-42.
84. Li P, Liu L, Xiao H, Zhang W, Wang L, Tang B. A new polymer nanoprobe based on chemiluminescence resonance energy transfer for ultrasensitive

imaging of intrinsic superoxide anion in mice. J Am Chem Soc. 2016; 138: 2893-6.
85. Bronsart LL, Stokes C, Contag CH. Chemiluminescence imaging of superoxide anion detects beta-cell function and mass. PLoS One. 2016; 11: e0146601.
86. Jie X, Yang H, Wang M, Zhang Y, Wei W, Xia Z. A peroxisome-Inspired chemiluminescent silica nanodevice for the intracellular detection of biomarkers and its application to insulin-sensitizer screening. Angew Chem Int Ed Engl. 2017; 56: 14596-601.
87. Ren H, Long Z, Cui M, Shao K, Zhou K, Ouyang J, et al. Dual-functional nanoparticles for in situ sequential detection and imaging of ATP and H_2O_2. Small. 2016; 12: 3920-4.
88. Lee ES, Deepagan VG, You DG, Jeon J, Yi GR, Lee JY, et al. Nanoparticles based on quantum dots and a luminol derivative: implications for in vivo imaging of hydrogen peroxide by chemiluminescence resonance energy transfer. Chem Commun. 2016; 52: 4132-5.
89. Hai Z, Li J, Wu J, Xu J, Liang G. Alkaline phosphatase-triggered simultaneous hydrogelation and chemiluminescence. J Am Chem Soc. 2017; 139: 1041-4.
90. Selvakumar LS, Thakur MS. Dipstick based immunochemiluminescence biosensor for the analysis of vitamin B-12 in energy drinks: a novel approach. Anal Chim Acta. 2012; 722: 107-13.
91. Vacher M, Fdez Galvan I, Ding BW, Schramm S, Berraud-Pache R, Naumov P, et al. Chemi- and bioluminescence of cyclic peroxides. Chem Rev. 2018; 118: 6927-74.
92. Chen Y, Spiering AJ, Karthikeyan S, Peters GW, Meijer EW, Sijbesma RP. Mechanically induced chemiluminescence from polymers incorporating a 1,2-dioxetane unit in the main chain. Nat Chem. 2012; 4: 559-62.
93. Cao J, Campbell J, Liu L, Mason RP, Lippert AR. In vivo chemiluminescent imaging agents for nitroreductase and tissue oxygenation. Anal Chem. 2016; 88: 4995-5002.
94. Hananya N, Eldar Boock A, Bauer CR, Satchi-Fainaro R, Shabat D. Remarkable enhancement of chemiluminescent signal by dioxetane-fluorophore conjugates: turn-on chemiluminescence probes with color modulation for sensing and imaging. J Am Chem Soc. 2016; 138: 13438-46.
95. Gnaim S, Green O, Shabat D. The emergence of aqueous chemiluminescence: new promising class of phenoxy 1,2-dioxetane luminophores. Chem Commun. 2018; 54: 2073-85.
96. Green O, Eilon T, Hananya N, Gutkin S, Bauer CR, Shabat D. Opening a gateway for chemiluminescence cell imaging: distinctive methodology for design of bright chemiluminescent dioxetane probes. ACS Cent Sci. 2017; 3: 349-58.
97. Hananya N, Green O, Blau R, Satchi-Fainaro R, Shabat D. A highly efficient chemiluminescence probe for the detection of singlet oxygen in living cells. Angew Chem Int Ed Engl. 2017; 56: 11793-6.
98. Green O, Gnaim S, Blau R, Eldar-Boock A, Satchi-Fainaro R, Shabat D. Near-infrared dioxetane luminophores with direct chemiluminescence emission mode. J Am Chem Soc. 2017; 139: 13243-8.
99. Roth-Konforti ME, Bauer CR, Shabat D. Unprecedented sensitivity in a probe for monitoring cathepsin B: chemiluminescence microscopy cell-imaging of a natively expressed enzyme. Angew Chem Int Ed Engl. 2017; 56: 15633-8.
100. Bruemmer KJ, Green O, Su TA, Shabat D, Chang CJ. Chemiluminescent probes for activity-based sensing of formaldehyde released from folate degradation in living mice. Angew Chem Int Ed Engl. 2018; 57: 7508-12.
101. Gnaim S, Scomparin A, Das S, Blau R, Satchi-Fainaro R, Shabat D. Direct real-time monitoring of prodrug activation by chemiluminescence. Angew Chem Int Ed Engl. 2018; 57: 9033-7.
102. Ni X, Zhang X, Duan X, Zheng H-L, Xue X-S, Ding D. Near-infrared afterglow luminescent aggregation-induced emission dots with ultrahigh tumor-to-liver signal ratio for promoted image-guided cancer surgery. Nano Lett. 2019; 19: 318-30.
103. Wilson T, Hastings JW. Bioluminescence. Annu Rev Cell Dev Biol. 1998; 14: 197-230.
104. de Wet JR, Wood KV, DeLuca M, Helinski DR, Subramani S. Firefly luciferase gene: structure and expression in mammalian cells. Mol Cell Biol. 1987; 7: 725-37.
105. Sun ML, Fu ZC, Wang T, Cui X, Dong J, Du F, et al. A high-throughput in vivo selection method for luciferase variants. Sens Actuators, B. 2018; 273: 191-7.
106. Godinat A, Bazhin AA, Goun EA. Bioorthogonal chemistry in bioluminescence imaging. Drug Discov Today. 2018; 23: 1584-90.
107. Jones KA, Porterfield WB, Rathbun CM, McCutcheon DC, Paley MA, Prescher JA. Orthogonal luciferase-luciferin pairs for bioluminescence imaging. J Am Chem Soc. 2017; 139: 2351-8.
108. Zou Y, Zhou Y, Jin Y, He C, Deng Y, Han S, et al. Synergistically enhanced antimetastasis effects by honokiol-loaded pH-sensitive polymer–doxorubicin conjugate micelles. ACS Appl Mater Interfaces. 2018; 10: 18585-600.
109. Iwano S, Sugiyama M, Hama H, Watakabe A, Hasegawa N, Kuchimaru T, et al. Single-cell bioluminescence imaging of deep tissue in freely moving animals. Science. 2018; 359: 935-9.
110. Mehle A. Fiat luc: bioluminescence imaging reveals in vivo viral replication dynamics. PLoS Pathog. 2015; 11: e1005081.
111. Hall MP, Woodroofe CC, Wood MG, Que I, van't Root M, Ridwan Y, et al. Click beetle luciferase mutant and near infrared naphthyl-luciferins for improved bioluminescence imaging. Nat Commun. 2018; 9: 132.
112. Wu N, Rathnayaka T, Kuroda Y. Bacterial expression and re-engineering of Gaussia princeps luciferase and its use as a reporter protein. Biochim Biophys Acta Proteins Proteomics. 2015; 1854: 1392-9.
113. Da-Som K, Jeong-Ran C, Jeong-Ae K, Kangmin K. Re-engineering of Bacterial Luciferase; for new aspects of bioluminescence. Curr Protein Pept Sci. 2018; 19: 16-21.
114. Yang Y, Shao Q, Deng R, Wang C, Teng X, Cheng K, et al. In vitro and in vivo uncaging and bioluminescence imaging by using photocaged upconversion nanoparticles. Angew Chem Int Ed Engl. 2012; 51: 3125-9.
115. Kamkaew A, Sun H, England CG, Cheng L, Liu Z, Cai W. Quantum dot-NanoLuc bioluminescence resonance energy transfer enables tumor imaging and lymph node mapping in vivo. Chem Commun. 2016; 52: 6997-7000.
116. Feugang JM, Youngblood RC, Greene JM, Willard ST, Ryan PL. Self-illuminating quantum dots for non-invasive bioluminescence imaging of mammalian gametes. J Nanobiotechnol. 2015; 13: 38.
117. Hattori M, Kawamura G, Kojima R, Kamiya M, Urano Y, Ozawa T. Confocal bioluminescence imaging for living tissues with a caged substrate of luciferin. Anal Chem. 2016; 88: 6231-8.
118. Kim TJ, Turkcan S, Pratx G. Modular low-light microscope for imaging cellular bioluminescence and radioluminescence. Nat Protoc. 2017; 12: 1055-76.
119. Kuruppu D, Brownell AL, Shah K, Mahmood U, Tanabe KK. Molecular imaging with bioluminescence and PET reveals viral oncolysis kinetics and tumor viability. Cancer Res. 2014; 74: 4111-21.
120. Ozawa T, Yoshimura H, Kim SB. Advances in fluorescence and bioluminescence imaging. Anal Chem. 2013; 85: 590-609.
121. Suff N, Waddington SN. The power of bioluminescence imaging in understanding host-pathogen interactions. Methods. 2017; 127: 69-78.
122. Tung JK, Berglund K, Gutekunst CA, Hochgeschwender U, Gross RE. Bioluminescence imaging in live cells and animals. Neurophotonics. 2016; 3: 025001.
123. Paley MA, Prescher JA. Bioluminescence: a versatile technique for imaging cellular and molecular features. Medchemcomm. 2014; 5: 255-67.
124. Kim JE, Kalimuthu S, Ahn BC. In vivo cell tracking with bioluminescence imaging. Nucl Med Mol Imaging. 2015; 49: 3-10.
125. Badr CE, Tannous BA. Bioluminescence imaging: progress and applications. Trends Biotechnol. 2011; 29: 624-33.
126. Keyaerts M, Caveliers V, Lahoutte T. Bioluminescence imaging: looking beyond the light. Trends Mol Med. 2012; 18: 164-72.
127. Hochgrafe K, Mandelkow EM. Making the brain glow: in vivo bioluminescence imaging to study neurodegeneration. Mol Neurobiol. 2013; 47: 868-82.
128. Hardy J, Selkoe DJ. The amyloid hypothesis of Alzheimer's disease: progress and problems on the road to therapeutics. Science. 2002; 297: 353-6.
129. Watts JC, Giles K, Grillo SK, Lemus A, Dearmond SJ, Prusiner SB. Bioluminescence imaging of Aβ deposition in bigenic mouse models of Alzheimer's disease. Proc Natl Acad Sci U S A. 2011; 108: 2528-33.
130. Liu L, Mason RP, Gimi B. Dynamic bioluminescence and fluorescence imaging of the effects of the antivascular agent Combretastatin-A4P (CA4P) on brain tumor xenografts. Cancer Lett. 2015; 356: 462-9.
131. Aelvoet SA, Ibrahimi A, Macchi F, Gijsbers R, Van den Haute C, Debyser Z, et al. Noninvasive bioluminescence imaging of alpha-synuclein oligomerization in mouse brain using split firefly luciferase reporters. J Neurosci. 2014; 34: 16518-32.
132. Kono M, Conlon EG, Lux SY, Yanagida K, Hla T, Proia RL. Bioluminescence imaging of G protein-coupled receptor activation in living mice. Nat Commun. 2017; 8: 1163.
133. Taylor MC, Kelly JM. Optimizing bioluminescence imaging to study protozoan parasite infections. Trends Parasitol. 2014; 30: 161-2.
134. Branchini BR, Southworth TL, Fontaine DM, Kohrt D, Talukder M, Michelini E, et al. An enhanced chimeric firefly luciferase-inspired enzyme for ATP detection and bioluminescence reporter and imaging applications. Anal Biochem. 2015; 484: 148-53.
135. Adams ST, Jr., Mofford DM, Reddy GS, Miller SC. Firefly luciferase mutants allow substrate-selective bioluminescence imaging in the mouse brain. Angew Chem Int Ed Engl. 2016; 55: 4943-6.
136. Maguire CA, Bovenberg MS, Crommentuijn MH, Niers JM, Kerami M, Teng J, et al. Triple bioluminescence imaging for in vivo monitoring of cellular processes. Mol Ther Nucleic Acids. 2013; 2: e99.
137. Takaku Y, Murai K, Ukai T, Ito S, Kokubo M, Satoh M, et al. In vivo cell tracking by bioluminescence imaging after transplantation of bioengineered cell sheets to the knee joint. Biomaterials. 2014; 35: 2199-206.
138. Isomura A, Ogushi F, Kori H, Kageyama R. Optogenetic perturbation and bioluminescence imaging to analyze cell-to-cell transfer of oscillatory information. Genes Dev. 2017; 31: 524-35.
139. Merritt J, Senpuku H, Kreth J. Let there be bioluminescence: development of a biophotonic imaging platform for in situ analyses of oral biofilms in animal models. Environ Microbiol. 2016; 18: 174-90.
140. Yasunaga M, Nakajima Y, Ohmiya Y. Dual-color bioluminescence imaging assay using green- and red-emitting beetle luciferases at subcellular resolution. Anal Bioanal Chem. 2014; 406: 5735-42.
141. Cevenini L, Camarda G, Michelini E, Siciliano G, Calabretta MM, Bona R, et al. Multicolor bioluminescence boosts malaria research: quantitative dual-color assay and single-cell imaging in Plasmodium falciparum parasites. Anal Chem. 2014; 86: 8814-21.

142. Daniel C, Poiret S, Dennin V, Boutillier D, Pot B. Bioluminescence imaging study of spatial and temporal persistence of Lactobacillus plantarum and Lactococcus lactis in living mice. Appl Environ Microbiol. 2013; 79: 1086-94.
143. Jathoul AP, Grounds H, Anderson JC, Pule MA. A dual-color far-red to near-infrared firefly luciferin analogue designed for multiparametric bioluminescence imaging. Angew Chem Int Ed Engl. 2014; 53: 13059-63.
144. Feng P, Zhang H, Deng Q, Liu W, Yang L, Li G, et al. Real-time bioluminescence imaging of nitroreductase in mouse model. Anal Chem. 2016; 88: 5610-4.
145. Aron AT, Heffern MC, Lonergan ZR, Vander Wal MN, Blank BR, Spangler B, et al. In vivo bioluminescence imaging of labile iron accumulation in a murine model of Acinetobacter baumannii infection. Proc Natl Acad Sci U S A. 2017; 114: 12669-74.
146. Ke B, Ma L, Kang T, He W, Gou X, Gong D, et al. In vivo bioluminescence imaging of cobalt accumulation in a mouse model. Anal Chem. 2018; 90: 4946-50.
147. Tian X, Liu X, Wang A, Lau C, Lu J. Bioluminescence imaging of carbon monoxide in living cells and nude mice based on Pd^0-mediated Tsuji-Trost reaction. Anal Chem. 2018; 90: 5951-8.
148. Zhang M, Wang L, Zhao Y, Wang F, Wu J, Liang G. Using bioluminescence turn-on to detect cysteine in vitro and in vivo. Anal Chem. 2018; 90: 4951-4.
149. Yuan Y, Liang G. A biocompatible, highly efficient click reaction and its applications. Org Biomol Chem. 2014; 12: 865-71.
150. Van de Bittner GC, Bertozzi CR, Chang CJ. Strategy for dual-analyte luciferin imaging: in vivo bioluminescence detection of hydrogen peroxide and caspase activity in a murine model of acute inflammation. J Am Chem Soc. 2013; 135: 1783-95.
151. Fu Q, Duan X, Yan S, Wang L, Zhou Y, Jia S, et al. Bioluminescence imaging of caspase-3 activity in mouse liver. Apoptosis. 2013; 18: 998-1007.
152. McCutcheon DC, Paley MA, Steinhardt RC, Prescher JA. Expedient synthesis of electronically modified luciferins for bioluminescence imaging. J Am Chem Soc. 2012; 134: 7604-7.
153. Sun YQ, Liu J, Wang P, Zhang J, Guo W. D-luciferin analogues: a multicolor toolbox for bioluminescence imaging. Angew Chem Int Ed Engl. 2012; 51: 8428-30.
154. Mezzanotte L, van 't Root M, Karatas H, Goun EA, Lowik C. In vivo molecular bioluminescence imaging: new tools and applications. Trends Biotechnol. 2017; 35: 640-52.
155. Adams ST, Jr., Miller SC. Beyond D-luciferin: expanding the scope of bioluminescence imaging in vivo. Curr Opin Chem Biol. 2014; 21: 112-20.
156. Wu W, Su J, Tang C, Bai H, Ma Z, Zhang T, et al. cybLuc: An effective aminoluciferin derivative for deep bioluminescence imaging. Anal Chem. 2017; 89: 4808-16.
157. Evans MS, Chaurette JP, Adams ST, Jr., Reddy GR, Paley MA, Aronin N, et al. A synthetic luciferin improves bioluminescence imaging in live mice. Nat Methods. 2014; 11: 393-5.
158. Kuchimaru T, Iwano S, Kiyama M, Mitsumata S, Kadonosono T, Niwa H, et al. A luciferin analogue generating near-infrared bioluminescence achieves highly sensitive deep-tissue imaging. Nat Commun. 2016; 7: 11856.
159. Takakura H, Kojima R, Ozawa T, Nagano T, Urano Y. Development of 5'- and 7'-substituted luciferin analogues as acid-tolerant substrates of firefly luciferase. ChemBioChem. 2012; 13: 1424-7.
160. Steinhardt RC, O'Neill JM, Rathbun CM, McCutcheon DC, Paley MA, Prescher JA. Design and synthesis of an alkynyl luciferin analogue for bioluminescence imaging. Chem--Eur J. 2016; 22: 3671-5.
161. Mofford DM, Jr AS, Reddy GS, Reddy GR, Miller SC. Luciferin amides enable in vivo bioluminescence detection of endogenous fatty acid amide hydrolase activity. J Am Chem Soc. 2015; 137: 8684-7.
162. Yuan Y, Wang F, Tang W, Ding Z, Wang L, Liang L, et al. Intracellular self-assembly of cyclic D-luciferin nanoparticles for persistent bioluminescence imaging of fatty acid amide hydrolase. ACS Nano. 2016; 10: 7147-53.
163. Lohse MJ, Nuber S, Hoffmann C. Fluorescence/bioluminescence resonance energy transfer techniques to study G-protein-coupled receptor activation and signaling. Pharmacol Rev. 2012; 64: 299-336.
164. Dragulescuandrasi A, Chan CT, De A, Massoud TF, Gambhir SS. Bioluminescence resonance energy transfer (BRET) imaging of protein-protein interactions within deep tissues of living subjects. Proc Natl Acad Sci U S A. 2011; 108: 12060-5.
165. Xiong L, Shuhendler AJ, Rao J. Self-luminescing BRET-FRET near-infrared dots for in vivo lymph-node mapping and tumour imaging. Nat Commun. 2012; 3: 1193.
166. Chu J, Oh Y, Sens A, Ataie N, Dana H, Macklin JJ, et al. A bright cyan-excitable orange fluorescent protein facilitates dual-emission microscopy and enhances bioluminescence imaging in vivo. Nat Biotechnol. 2016; 34: 760-7.
167. Yeh HW, Karmach O, Ji A, Carter D, Martins-Green MM, Ai HW. Red-shifted luciferase-luciferin pairs for enhanced bioluminescence imaging. Nat Methods. 2017; 14: 971-4.
168. Yuan H, Chong H, Wang B, Zhu C, Liu L, Yang Q, et al. Chemical molecule-induced light-activated system for anticancer and antifungal activities. J Am Chem Soc. 2012; 134: 13184-7.
169. Lecuyer T, Teston E, Ramirez-Garcia G, Maldiney T, Viana B, Seguin J, et al. Chemically engineered persistent luminescence nanoprobes for bioimaging. Theranostics. 2016; 6: 2488-524.
170. Liu J, Lecuyer T, Seguin J, Mignet N, Scherman D, Viana B, et al. Imaging and therapeutic applications of persistent luminescence nanomaterials. Adv Drug Deliv Rev. 2019; 138: 193-210.